ELSEVIER

Remote Sensing of Environment

Testing a LiSK BRDF Model with in Situ Bidirectional Reflectance Factor Measurements over Semiarid Grasslands

*Mark J. Chopping**

The non-Lambertian nature of the terrestrial surface is a major source of unexplained variability in wide-swath satellite sensor data acquired in the solar reflective wavelengths, hindering quantitative analysis in the spectral, temporal, and locational domains. The interactions of light with the surface are governed by the bidirectional reflectance distribution function (BRDF), and modeling this is one of the most promising methods for describing and explaining this variability. Here the Roujean linear semiempirical kernel-driven (LiSK) model was tested against two independent bidirectional reflectance factor datasets that were acquired close to ground level over seminatural semiarid grasslands in Xilingol, Inner Mongolia (People's Republic of China) and in Arizona (United States). The objectives were to determine how well the model is able to describe and explain observed bidirectional reflectance factor distributions in the red and near-infrared wavelengths, to explore its utility in correcting such data for angular variations, and the likely impact of such corrections on cover-type discrimination. The sensitivity of the model to reductions in the number and angular distribution of the bidirectional reflectance observations with which it is inverted was also evaluated. The results show that the model is able to describe the observed multiangular BRFs with good accuracy and with low sensitivity to the number of angular inputs, with observations in the forward-scattering direction shown to be important in constraining inversions. The behavior of retrieved parameters indicates that one or more of the simplifying assumptions made in the model derivation is likely to be too severe for explaining BRDF in the near-infrared region; non-negligible anisotropic multiple scattering and the assumption of an optically thick medium mean that a physical interpretation of parameters is unlikely to be valid. However, the model is shown to provide an effective means of correcting for BRDF effects, allowing greater precision and consistency than hitherto possible in the retrieval of surface spectral reflectance over semiarid grasslands and concrete improvements in cover-type discrimination. Published by Elsevier Science Inc.

INTRODUCTION

Multiangular bidirectional reflectance factors (BRFs) obtained in situ are useful in remote sensing research since atmospheric path radiance is removed from the signal, enabling testing of bidirectional reflectance distribution function (BRDF) models in a relatively controlled manner. The BRDF is a fundamental and intrinsic physical property that governs the reflectance behavior of a surface, for which a spectral dependence is observed. BRDF models are required to correct remotely sensed data for angular effects, to determine surface shortwave albedo via prediction of reflectance at a wide range of sun-target-sensor geometries, and to provide surface information—whether semiempirical or physical—which is not available in the spectral, temporal, or locational domains (Diner et al., 1999). If any one of the sources of variation (spectral, temporal, locational, directional) is not adequately accounted for, then the use of the others is compromised: there will be unexplained variation in the data. Although the BRDF can never be measured directly, multidirectional measurements can provide useful estimates of it. Field BRF measurements are not truly bidirectional, because incoming solar radiation does not have a unique direction but rather an angular distribution determined by the turbidity of the atmosphere (Guyot, 1990).

* USDA-ARS Hydrology Laboratory, Beltsville Agricultural Research Center-West

Address correspondence to Mark J. Chopping, USDA-ARS Hydrology Laboratory, Beltsville Agricultural Research Center-West, Beltsville, MD 20705, USA. E-mail: chopping@hydrolab.arsusda.gov

Received 8 November 1999; revised 17 March 2000.

REMOTE SENS. ENVIRON. 74:287–312 (2000)
Published by Elsevier Science Inc.
655 Avenue of the Americas, New York, NY 10010

0034-4257/00/$–see front matter
PII S0034-4257(00)00122-X

For narrow instantaneous field-of-view (IFOV) radiometers the term "bidirectional reflectance factor" is deemed appropriate.

The literature reveals that BRDF model evaluations are often carried out using data simulated with other models (Pinty and Verstraete, 1991; Hesley et al., 1996; Asner et al., 1997; Hyman and Wanner, 1997; Walthall, 1997; Engelsen et al., 1997; Iaquinta and Fouilloux, 1998). While this is a useful means for testing certain aspects of model behavior, there is always the question of the reliability of the reference model. Bidirectional reflectance data are retrievable from space-borne sensors, although these data may be degraded in rather specific ways by imperfect calibration, residual contamination from atmospheric scattering and absorption, and restricted temporal and directional viewing. On the other hand, bidirectional reflectance data acquired in the laboratory are often restricted to a small number of components, such as soil samples, individual plants, or small uniform groupings, and it is almost impossible to recreate in the laboratory the complex mixture of elements that together make up real terrestrial surfaces (Curran and Kupiec, 1995). Some advances have been made in this area with field goniometers (Sandmeier and Itten, 1999), although such techniques are still limited to low canopies, such as grasslands with annuals and very low shrubs; for higher shrub canopies instruments such as the PARABOLA must be used (Deering and Leone, 1986; Middleton et al., 1987). For these reasons, surface bidirectional reflectance factor measurements derived in situ from spectral radiance observations close to ground level are useful in assessing BRDF models' capabilities in describing or explaining the anisotropies of existing complex heterogeneous surfaces.

The validation of BRDF models for semiarid grassland sites like those investigated here is important since the locations are representative of a terrestrial surface type that accounts for a large proportion of the total global land area: arid and semiarid ecosystems (e.g., savannas, shrublands, and grasslands) constitute about 41% (53 million km^2) of the terrestrial surface, covering vast areas of the African (60%), North and South American (45%), Australian (65%), and Asian (30%) continents (Matthews, cited in Asner et al. 1998; Schlesinger et al., 1990). The ability to determine rates of change in biophysical and geophysical parameters, such as albedo, cover, canopy height, and leaf area index (LAI), on a regional and global basis from remotely sensed data is a prerequisite for many important applications, including climate modeling and the assessment of the impact of human-induced degradation on dryland ecosystems. These are marginal environments and climate- and human-induced degradation can result in invasion by unproductive species and a loss of productive capacity of a type considered beneficial to mankind. There is generally a high level of susceptibility to climate change and population pressure (Huete et al., 1994). The implications for the global energy budget are of great importance since soils in these regions are bright throughout the visible to near-infrared (NIR) region.

In this study field bidirectional reflectance data from test sites in Inner Mongolia Autonomous Region (People's Republic of China) and Walnut Gulch, Arizona (United States) are used to test the semiempirical model of Roujean et al. (1992a). This model, hereafter referred to as the "Roujean model," was selected for use with data from the POLDER (Polarisation and Directionality of Earth's Reflectance) sensor on NASDA's ADEOS satellites (Deschamps et al., 1994), and because its form has become the basis for a suite of BRDF models collectively known as AMBRALS (Algorithm for MODIS Bidirectional Reflectance Anisotropy of the Land Surface), which was designed for the production of the global BRDF/Albedo product from the MODIS and MISR sensors on NASA's Terra satellite (Strahler et al., 1996). It has been found to perform rather well in other evaluations when fitted to bidirectional reflectance data from the surface (Kimes, 1983; Kimes et al., 1985; Kimes et al., 1986); from the air (Leroy and Bréon, 1996; Barnsley et al., 1997b; Disney et al., 1997; Lewis et al., 1998); and from space (Roujean et al., 1992b; Wu et al., 1995; Li et al., 1996; Disney et al., 1997; Vives Ruiz de Lope and Lewis, 1997). The model is referred to here as a *Li*near *S*emiempirical *K*ernel-driven (LiSK) model: it is linear with respect to its parameters; it is semiempirical in that a partitioning of the surface reflectance anisotropy into geometric and volume components is assumed; and it is kernel-driven in that separate functions for geometric-optical and volume scattering are developed. Important assumptions are made to simplify physical terms so that a tractable formulation is obtained. The ancestry of this type of model includes the formulation of the Walthall model (Walthall et al., 1985; Walthall, 1997) and the turbid, medium volume scattering functions of Ross (1981), which are combined here with an original geometric scattering function. Preliminary results from Roujean model inversions with data from the POLDER sensor flown on aircraft and onboard the first ADEOS satellite were reported to be promising (Hautecoeur and Leroy, 1998). Validation over a wide range of terrestrial surfaces and with different BRDF sampling constraints is required to test whether the model performs as intended: even when reasonable parameters are retrieved, it is still not certain that they contain only physical quantities since when the geometric-optical and volume scattering kernels are inverted simultaneously, one or the other may become unreliable (Disney and Lewis, 1998).

BRDF models have not been routinely applied in off-nadir satellite data processing, partly because there has been a lack of adequate multiangular data; partly because the models available could not describe or explain BRDF with sufficient accuracy, reliability, generality, and rapidity for operational use; and partly because of a general lack of appreciation of the impact of the non-Lambertian properties of terrestrial surfaces on spectral radiance measure-

ments. All three factors have been addressed more fully in recent years, and it has become apparent that LiSK BRDF models may be suitable for operational use in that according to their formulation they should have the constructive properties described by Roujean et al. (1992a), Barnsley et al. (1997a), and Wanner et al. (1995). Disadvantages of LiSK BRDF models include the inability to directly provide biophysical parameters; the requirement for observations close to the principal plane and in both back- and forward-scattering directions (although this may also apply to other model types); lack of terms to account for behavior at the hot spot (Kuusk, 1991), specular scattering effects, and low-order multiple scattering phenomena; some level of inaccuracy in predicting BRDF in unobserved regions when the angular sampling is suboptimal; and the possibility of model misbehavior and retrieval of unphysical or unreasonable parameters.

OBJECTIVES

The primary objective of this study was to determine how far the Roujean model is able to describe and explain the observed azimuthal bidirectional reflectance factor distributions in the red and NIR wavelengths obtained for contrasting grassland canopy types, using surface parameters derived from model fits to in situ measurements at a range of view and illumination geometries. A further objective was to explore the utility of the model in reducing the directional dependency in the observed bidirectional reflectance factors and the impact of such corrections on cover-type discrimination. This depends only on the model's ability to describe the BRDFs of these grasslands. An important part of the tests is the evaluation of the retrieved surface parameters (kernel weights). Since the model is based on a simplification of the physics of the interaction of radiation in the solar reflective wavelengths with partly vegetated surfaces, it is hypothesized that the anisotropic model surface parameters should yield some relationship to the three-dimensional (structural) characteristics of green canopies, such as canopy height and foliage density. The validity of such relationships and the feasibility of a "model-to-model" approach (Qi et al., 1995) depends on the ability to at least partly explain BRDF, rather than the ability merely to describe it. Finally, the stability of the model is investigated with respect to both model fit and the robustness of the surface parameters with variation in the number and angular distribution of observations.

METHODS

Inner Mongolia Study Area and Field Sites

The field data used here were acquired in Xilingol league on the Inner Mongolia plateau at the peak of the growing season (August 1996), near Huhehaote, Inner Mongolia (late August/early September 1996) and at the Walnut Gulch Kendall North site, Arizona (June and August, 1990). The main study area is a semiarid grassland biome in Xilingol Aimag (League), Inner Mongolia Autonomous Region, Peoples' Republic of China. It is enclosed by the geographic coordinates 112.400°–116.051°E by 42.843°–44.711°N. The grasslands of Xilingol aimag are located on the Mongolian plateau, a vast high plain of greater than 1,000 m in altitude. These grasslands were formed during the early Oligocene–early Pleistocene, and there is evidence to suggest that since the late Holocene the aridity of the physical environment has shifted toward the east (Xiao et al., 1993). These grasslands are classed as semiarid, meaning that annual rainfall is between 250 mm and 400 mm. More than 80% of total annual precipitation falls in July and August, which is the peak of the growing season. As is common with other semiarid grasslands, precipitation and vegetation growth are highly variable both temporally and spatially. The growing season is generally short; much of the region is snow-covered from late October to early April. Temperature extremes lower than −30°C are common in January, the coldest month. The warmest month is July, with monthly average temperatures of between 16°C to 26°C over the entire region.

The study area encompasses a variety of grassland types from sparsely vegetated short *Stipa gobica* desert steppe (over bright sandy soils) to lush climax *Stipa grandi/Aneurolipideum chinense* "typical" steppe with a maximum canopy height of 1 m (over chestnut soils). Relief is generally not important with only gently rolling hills, and there is a variety of land uses from salt extraction to fodder production. There are recognized problems of land degradation, with increasing pressure on the steppe environment on both anthropogenic and climatic fronts. The issue of topography is particularly important since most BRDF modeling approaches assume a flat, horizontal terrain (Privette et al., 1997). Table 1 lists the sites, dates, and times at which angular radiometric measurements were taken, together with other vegetation and soil information. It should be noted that the summer of 1996 was a particularly wet season in central Inner Mongolia, with sporadic but unusually important rainfall events at intervals in both July and August. Vegetation cover estimates were derived from classifications of color photographs taken in situ at 4 m above the surface. For LAI estimates, all vegetation was cut from an area of 1.74 m^2 (corresponding to the 100% field of view of the radiometer), spread as evenly as possible on a large, light-colored plastic sheet, and two nadir photographs were taken from 2.8 m. LAI estimates were made through sorting the lookup table of the scanned images by hue.

Reflectance Factor Datasets

Bidirectional reflectance factor datasets from two semiarid grasslands are used: one from Inner Mongolia, acquired by a team led by the author, and one from Arizona, acquired as part of the Monsoon '90 watershed experiment (Kustas

Table 1. Main Characteristics of the 1996 Inner Mongolia Off-Nadir Radiometry Sites

Site Code	*Grassland Type*	*Dominant Species*	*DOY*	*TOD (LST)*[a]	*SZA* (°)	*Cover (%)*[b]	*Height (cm)*	*Fresh Weight*[c]	*LAI*	*Soil Color*[d]	*Soil pH*
A2	D. steppe	*Stipa gobica*	218	2.47	38.5	45	16	79	0.14	10YR 5/4	11.0
A8	D. steppe	*Stipa gobica/krylovii*	219	4.03	57.4	58	65	74	0.31	10YR 4/4	7.5
B9	D. steppe	*Caragana microphylla*	223	2.40	44.3	53	26	150	0.22	7.5YR 4/4	10.0
C4	T. steppe	*A. frigida/Carex sp.*	226	3.25	48.6	67	40	300	0.33	5YR 4/3	8.4
D7	T. steppe	*Stipa grandis*	231	3.15	49.9	76	95	580	0.36	10YR 4/3	8.2
D8	T. steppe	*Stipa grandis*	231	4.10	61.8	79	85	600	0.45	10YR 4/3	8.0
F5	T. steppe	*A. chinense*[e]	235	2.00	39.9	74	60	650	0.84	10YR 3/2	7.2
G9	D-T. ecotone	*Neopallasia pectinata*	236	2.45	45.2	49	40	240	0.42	7.5YR 5/4	7.6
Z	Grazed pasture	*Carex spp.*	242	4.30	63.6	74	10	180	na	na	na
Y	Forb patch	*Artemisia spp.*	252	5.00	74.6	83	60	600	na	na	na

D.=desert; T.=typical; D-T.=desert-typical; na=not available; SZA=solar zenith angle; LAI=leaf area index, derived via classification of nadir photography of vegetation samples.

[a] Time of day (Local Solar Time). All readings were done in the afternoon.

[b] Cover estimates calculated by classified nadir photography at 4 m with shadow allocated on the basis of the initial soil/vegetation breakdown. Height is maximum height of dominant species at each site.

[c] Fresh weight (g/1.74 m^2).

[d] Munsell system.

[e] Aneurolipideum chinense.

and Goodrich, 1994). Data from the Monsoon '90 Experiment (Walnut Gulch Kendall North site) for DOY 156 and DOY 220 were selected to provide a check on the Inner Mongolia data since the study is well-documented, and climate and vegetation characteristics are broadly similar. For the Inner Mongolia experiments, bidirectional reflectance factor measurements were taken at the peak of the 1996 growing season for a variety of grassland landscapes of homogeneous composition on the Inner Mongolian plateau (sites denominated A to G) and near the regional capital Huhehaote (sites denominated Y and Z) using a Milton Multiband radiometer. First introduced in 1978 as a low-cost field-portable radiometer sensing in the four Landsat MSS bands, the Milton Multiband Radiometer used here is an improved version with silicon photodiode detectors. Measurements of target and reference are taken simultaneously ("dual beam simultaneous mode") to avoid the problem of rapidly changing illumination. The two sensors were fitted with filters for green, red, near-infrared (NIR), and middle-infrared (MIR) wavelengths, corresponding roughly to TM2, TM3, TM4, and TM5 bands of the Landsat Thematic Mapper. Since the detectors are linear in their response to incoming flux, this allows a simple intercalibration to be accomplished. The spectral response of the detectors in the solar wavelengths and the reflectivity of the bright white, pressed halon reference panel are shown in Figure 1.

Prior to field use, a sensor head intercalibration factor was calculated by least squares regression on a sample of measurements from both surface and reference sensors viewing the same area of a light-colored concrete surface under varying illumination conditions. Correlation coefficients of 0.998 to 1.00 were obtained between the two sensors' outputs. The sensor mast was extended vertically from 2.8 m to 4.0 m to increase the area of surface visible to the sensor, so that a more representative sample of all surface components would be obtained, which is especially important for patchy surfaces. The mast was also extended horizontally, so that the base of the mast and the feet of survey personnel would not intrude into the sensor field-of-view. A 20×20×1.5-cm pressed halon reflectance panel was used as the reference surface at all sites, and dark level offset readings from the radiometer were taken several times during each day by thoroughly blocking out all light from both sensor heads. The offsets were rarely significant in relation to the surface readings. The reference panel sensor head was moved to a position approximately 2.5 m from the base of the radiometer mast to avoid shading by mast or staff, and any tall vegetation surrounding it was removed.

The nominal instantaneous field of view (IFOV) of the Milton radiometer is 15°, and for the Xilingol sites the distance to surface is 4 m; thus at the maximum tilt of 40°, the projected surface area of the IFOV becomes 2.84 m^2 with a major axis of 1.38 m. These values are for the nominal sensor IFOV, which at nadir represents a 50% concentration ellipse rather than the total surface area contributing to the measured radiance [i.e., it describes

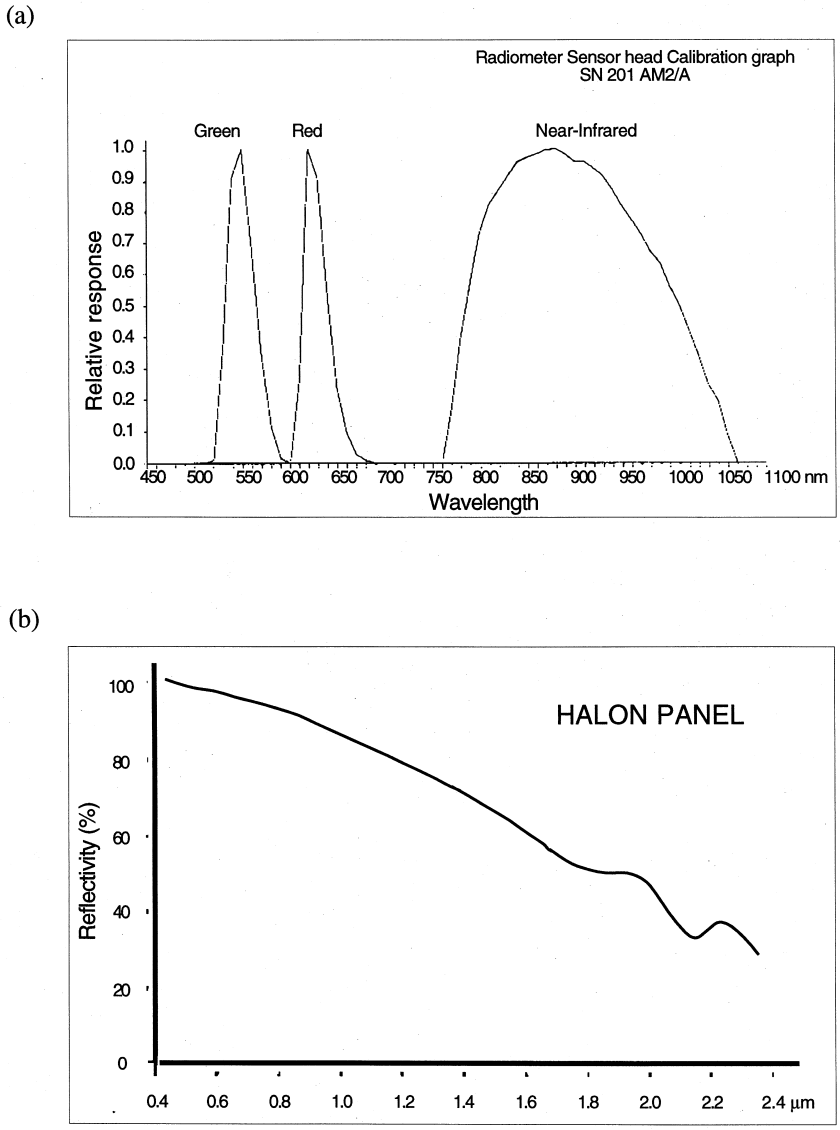

Figure 1. (a) Spectral response of Milton Multiband Radiometer channels 1, 2, and 3. (b) Reflectivity of pressed halon panel (%).

the area which accounts for 50% of incoming energy (Notes for Users, 1993)]. The point spread function of the sensor is such that the total surface area contributing to the measurements is approximately 1.74 m^2 at nadir with a projected IFOV diameter of 1.49 m; these values are 0.85 m^2 and 1.04 m for the Huhehaote sites, respectively, where a lower mast height of 2.8 m was used. The configuration of the two radiometers and mast for nadir view measurements is shown in Figures 2a and 2b. Off-nadir measurements were made between 2:00 P.M. and 4:30 P.M. LST (solar zenith angles from 38° to 62°) for view zenith angles ranging from 40° in the backscattering direction to 40° in the forward-scattering direction in increments of 10°, with the viewing plane oriented east–west and providing a range of relative azimuths from 11° to 48° (backscattering) and 132° to 169° (forward-scattering) (Fig. 2c). The geometry at site *Y* is exceptional with solar zenith angles of ~75° and view zenith angles in the range ±50°. For each view zenith angle, a pair of measurements were taken to provide an indication of instrument and environmental error (for example, the effects of wind and changing irradiance). No smoothing was carried out on the observed reflectance factors, for example, by fitting polynomial curves through the data points or averaging pairs of values. This provides a set of between 16 and 22 angular measurements for each site in each channel in a single azimuthal viewing plane. Each set of measurements took around 20 minutes to complete, and changes in solar zenith and azimuth angles are taken into account when fitting to the BRDF model. Bidirectional reflectance factors were calculated from the radiometry data assuming a quasi-Lambertian reflectance panel and using the relation shown in Eq. (1):

$$\text{reflectance factor (dimensionless)} = \frac{(V_s - V_p)}{(V_r - V_q)}(k)\ (h) \qquad (1)$$

where V_s and V_r are the meter reading from the target and

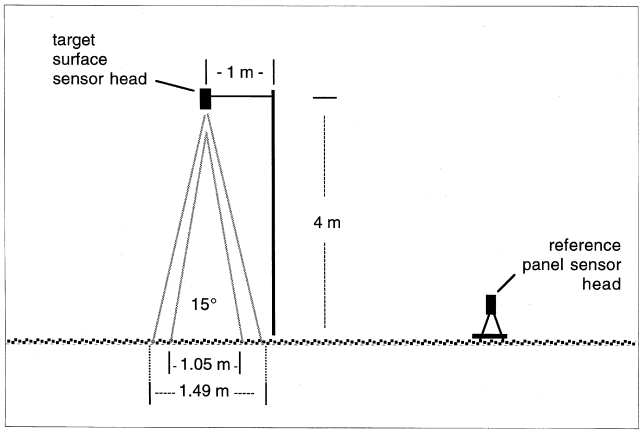

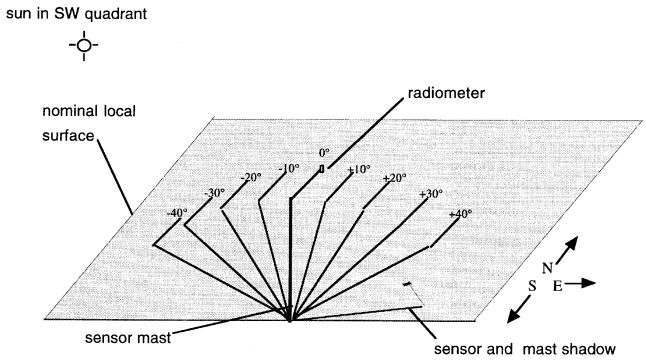

Figure 2. Configuration of Milton multispectral radiometers for nadir reflectance factor measurements: (top) Schematic, (middle) photograph of nadir radiometry in *Stipa gobica* desert steppe, and (bottom) schematic of radiometer tilting for BRF measurements.

reflectance panel in each channel, respectively; V_p and V_q are the dark level offset voltages for the target and panel sensor channels, respectively; k is the in-band reflectance factor of the reflectance panel; and h is the sensor head intercalibration factor.

The derivation of the Walnut Gulch (Arizona) datasets is documented in Huete et al. (1992), Moran et al. (1994), and Qi et al. (1994). The data were acquired over a semidesert gramma grassland (*Bouteloua* spp.) using a SE590 spectroradiometer mounted on a 2-m rotary arm, allowing the sensor to view the target at varying zenith angles from −40° (backscattering) to +40° (forward-scattering) at increments of 10° (Jackson et al., 1990). The viewing plane of the apparatus was fixed perpendicular to the SPOT overpass direction (i.e., 100° from true north, allowing data to be acquired at a range of azimuths during the day). Pairs of measurements were taken for each viewing angle and the values averaged, giving nine observations in total. The data used in this study are for DOY 156 (dry season; visibly senesced and dead material) and DOY 220 (wet season; 40% green grass cover) (Moran et al., 1994).

BRDF Model Description

Full details of the derivation of the Roujean model are given in Roujean et al. (1992a) and a summary is provided in Wanner et al. (1995). Briefly, it is expressed as shown in Eq. (2):

$$R(\theta_s,\theta_v,\varphi)=k_0+k_1\, f_1(\theta_s,\theta_v,\varphi)+k_2\, f_2(\theta_s,\theta_v,\varphi) \qquad (2)$$

where $R(\theta_s,\theta_v,\varphi)$ is the modeled bidirectional reflectance in a given channel for the solar zenith, view zenith, and relative azimuth angles θ_s,θ_v, and φ, respectively. The model kernels $f_1(\theta_s,\theta_v,\varphi)$ and $f_2(\theta_s,\theta_v,\varphi)$ are analytical functions of the solar and viewing angles derived via simplifying physical terms. Specifically, f_1 accounts for geometric scattering and shadowing, neglecting mutual shadowing of protrusions from the surface, while f_2 accounts for volume scattering from a discrete medium of randomly located facets, assuming the single scattering approximation, an isotropic facet distribution function, and an optically thick medium. This function is derived from Ross' (1981) approximation for large values of leaf area index, and the RossThick kernel developed in Wanner et al. (1995) is a linear scaling of it. It is largely dependent on LAI. The surface parameters k_0, k_1, and k_2 are theoretically dependent on the three-dimensional structure and optical properties of a canopy and its background. Specifically, k_0 should represent the bidirectional reflectance viewing a surface at nadir with the overhead sun ($\theta_s=\theta_v=0$), while k_1 and k_2 should measure the relative contributions of the geometric/shadowing and volume scattering components in total reflectance, respectively. A similar formulation and rationale underlie the kernel-driven models derived in Wanner et al. (1995) and are based on combinations of the Li geometric-optical (Li et al., 1994) and Ross volume scattering functions adapted for sparse and dense cases; note that surface scattering kernels are generally formulated to deplete reflectance, while volume scattering kernels generally enhance reflectance (Fig. 3). Here, the k_0, k_1, and k_2 surface parameters for each grassland type investigated were determined analytically via matrix inversion. The inversion criterion is the minimization of the absolute differences between the

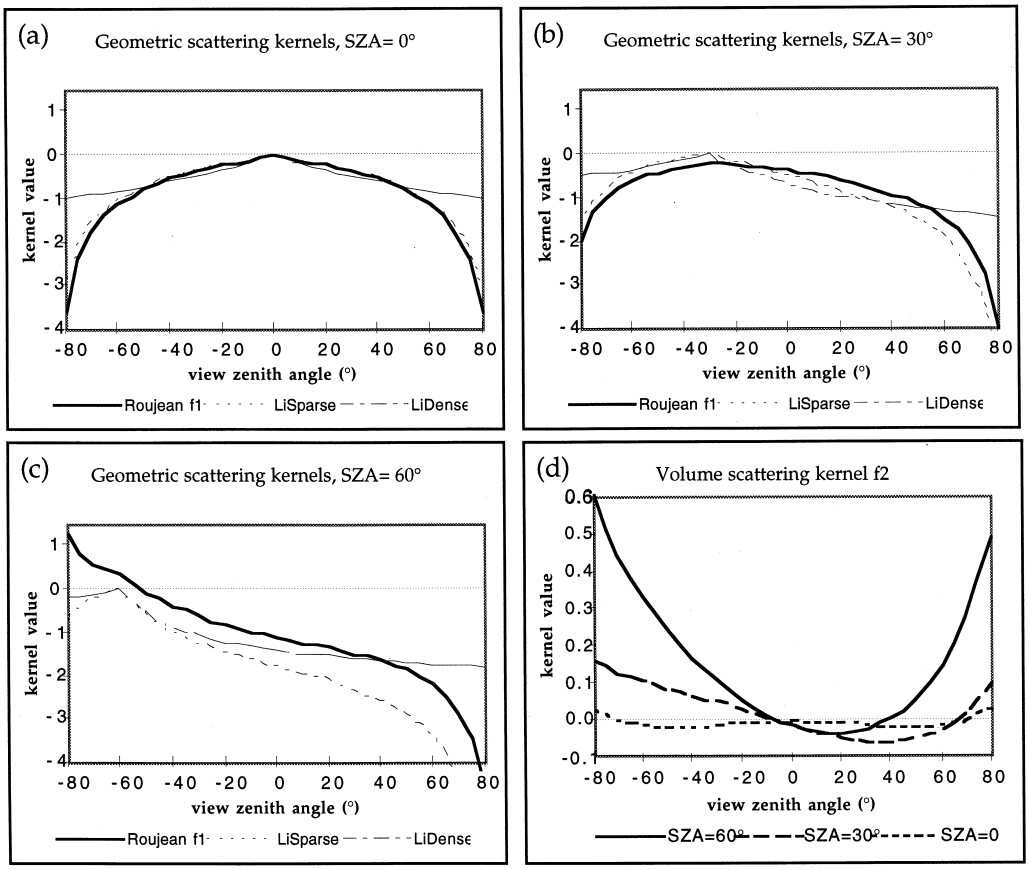

Figure 3. Anisotropic kernels: (a) geometric scattering kernels, solar zenith angle=0°; (b) geometric scattering kernels, solar zenith angle=30°; (c) geometric scattering kernels, solar zenith angle=60°; (d) volume scattering kernel for solar zenith angles of 0°, 30°, and 60°.

modeled and observed reflectance values in a given channel by attempting to minimize the (absolute) error term [see Eq. (3)]:

$$\partial^2 = 1/n \sum [(\rho_{\text{mod}})_i - (\rho_{\text{obs}})_i]^2 \qquad (3)$$

where ρ_{obs} is the observed reflectance, ρ_{mod} is modeled reflectance, n is the number of observations, and i is the channel.

An important function of BRDF models is the removal of directional dependency in angular reflectance data acquired at different illumination angles. Having determined the model surface parameters, an anisotropy factor Ω is calculated for each of the observed bidirectional reflectance values, by using Eq. (4) (Wu et al., 1995):

$$\Omega(\theta_s,\theta_v,\varphi) = R(\theta_s,\theta_v,\varphi)/(R(0,0,\varphi) = 1 + a_1 f_1(\theta_s,\theta_v,\varphi) + a_2 f_2(\theta_s,\theta_v,\varphi) \qquad (4)$$

where R is bidirectional spectral reflectance, $a_1 = k_1/k_0$, $a_2 = k_2/k_0$ and θ_s, θ_v, and φ are the solar zenith, view zenith, and relative azimuth angles, respectively. The anisotropy factors were used here to remove a proportion of the directional dependency in the observed reflectances by adjusting to a preferred geometry, by using Eq. (5):

$$R(\Theta_s,\Theta_v,\Phi) = [\Omega(\Theta_s,\Theta_v,\Phi)/\Omega(\theta_s,\theta_v,\varphi)] R(\theta_s,\theta_v,\varphi) \qquad (5)$$

where $R(\Theta_s,\Theta_v,\Phi)$ is the reflectance value in the desired geometry; $\Omega(\Theta_s,\Theta_v,\Phi)$ is the anisotropy factor for this desired configuration, calculated using the model k_0, k_1, and k_2 surface parameters; and $\Omega(\theta_s,\theta_v,\varphi)$ is the anisotropy factor for the measured reflectance in this channel. In this case the (arbitrary) preferred geometry was determined to be nadir viewing with the solar zenith as at the time of the nadir observations and in the principal plane.

RESULTS AND DISCUSSION

The main results of model inversions are presented in Tables 2 and 3, while Figures 4 to 7 show the observed, modeled, and normalized distributions for each set of red and NIR wavelength observations in Inner Mongolia and Arizona, respectively, where normalization means adjustment of angular reflectance to a chosen common view and illumination geometry. For the NIR channel, these tables and figures also include the corresponding results when the model is reduced to an isotropic component with a single anisotropic volume scattering kernel (right-hand columns); all discussion pertains to the original model unless otherwise indicated.

Table 2. Model Inputs, Model Fits, and Retrieved Parameters, Inner Mongolia

				NIR (with full model)					*NIR (with* $R=k_0+k_2f_2$*)*				*Red Channel*				
Site Code	*SZA (°)*	*RAA (°)*	*±VZA (°)*	k_0	k_1	k_2	*RMSE*	R^2	k_0	k_2	*RMSE*	R^2	k_0	k_1	k_2	*RMSE*	R^2
A2	39	33	40	0.320	0.004	0.336	0.004	0.93	0.318	0.350	0.004	0.93	0.229	0.038	0.130	0.005	0.90
A8	52	15	40	0.333	0.000	0.351	0.008	0.87	0.333	0.350	0.008	0.87	0.179	0.023	0.092	0.005	0.86
B9	39	35	40	0.341	−0.004	1.296	0.011	0.96	0.344	1.280	0.011	0.96	0.192	0.028	0.373	0.005	0.95
C4	49	23	40	0.350	−0.037	1.125	0.010	0.97	0.382	0.943	0.012	0.95	0.126	0.016	0.290	0.003	0.98
D7	50	26	40	0.190	−0.111	1.292	0.005	0.99	0.282	0.772	0.019	0.83	0.063	0.006	0.223	0.001	0.99
D8	62	13	40	0.143	−0.110	1.012	0.006	0.98	0.274	0.467	0.028	0.51	0.054	0.000	0.163	0.002	0.95
F5	38	48	40	0.180	−0.182	1.495	0.006	0.97	0.284	0.768	0.023	0.55	0.061	0.016	0.182	0.001	0.97
G9	45	36	40	0.253	−0.057	0.546	0.003	0.97	0.294	0.317	0.008	0.78	0.129	0.003	0.206	0.002	0.97
Z	62	14	40	0.316	−0.013	0.793	0.003	0.99	0.334	0.721	0.005	0.99	0.072	0.005	0.205	0.001	0.99
Y	75	11	50	0.280	−0.008	0.722	0.010	0.98	0.297	0.695	0.011	0.97	0.074	0.001	0.299	0.009	0.92

SZA=solar zenith angle; RAA=relative azimuth angle in backscattering half-space; VZA=view zenith angle; DOY=day of year; RMSE=root-mean-square error. Kernel weights: k_0=isotropic; k_1=geometric; k_2=volume scattering.

Table 3. Model Inputs, Model Fits, and Retrieved Parameters, Walnut Gulch Arizona

				NIR (with full model)					*NIR (with* $R=k_0+k_2f_2$*)*				*Red Channel*				
DOY	*SZA (°)*	*RAA (°)*	*±VZA (°)*	k_0	k_1	k_2	*RMSE*	R^2	k_0	k_2	*RMSE*	R^2	k_0	k_1	k_2	*RMSE*	R^2
156	50	10	40	0.250	0.018	0.701	0.006	0.98	0.235	0.785	0.007	0.98	0.189	0.018	0.512	0.004	0.99
156	43	14	40	0.243	−0.008	0.907	0.005	0.99	0.248	0.871	0.005	0.99	0.180	−0.003	0.676	0.003	0.99
156	16	21	40	0.252	0.018	0.749	0.006	0.93	0.246	0.837	0.006	0.92	0.194	0.019	0.647	0.005	0.92
156	9	79	40	0.249	0.016	1.127	0.003	0.91	0.248	1.495	0.003	0.90	0.193	0.015	1.033	0.002	0.94
220	65	14	40	0.204	−0.073	1.064	0.004	0.99	0.313	0.653	0.018	0.84	0.096	0.008	0.235	0.000	1.00
220	55	9	40	0.197	−0.100	1.129	0.006	0.98	0.295	0.643	0.017	0.84	0.097	0.009	0.280	0.001	1.00
220	43	0	40	0.199	−0.114	1.137	0.006	0.98	0.272	0.620	0.015	0.85	0.131	0.069	0.234	0.002	1.00
220	24	25	40	0.226	−0.065	0.820	0.002	0.99	0.251	0.549	0.008	0.85	0.106	0.016	0.339	0.001	0.99
220	23	29	40	0.190	−0.090	0.711	0.002	0.98	0.224	0.333	0.011	0.49	0.082	0.001	0.272	0.001	0.99
220	15	76	40	0.220	−0.048	0.737	0.001	0.95	0.231	0.046	0.005	0.00	0.097	0.009	0.513	0.000	0.99

SZA=solar zenith angle; RAA=relative azimuth angle in backscattering half-space; VZA=view zenith angle; DOY=day of year; RMSE=root-mean-square error. Kernel weights: k_0=isotropic; k_1=geometric; k_2=volume scattering.

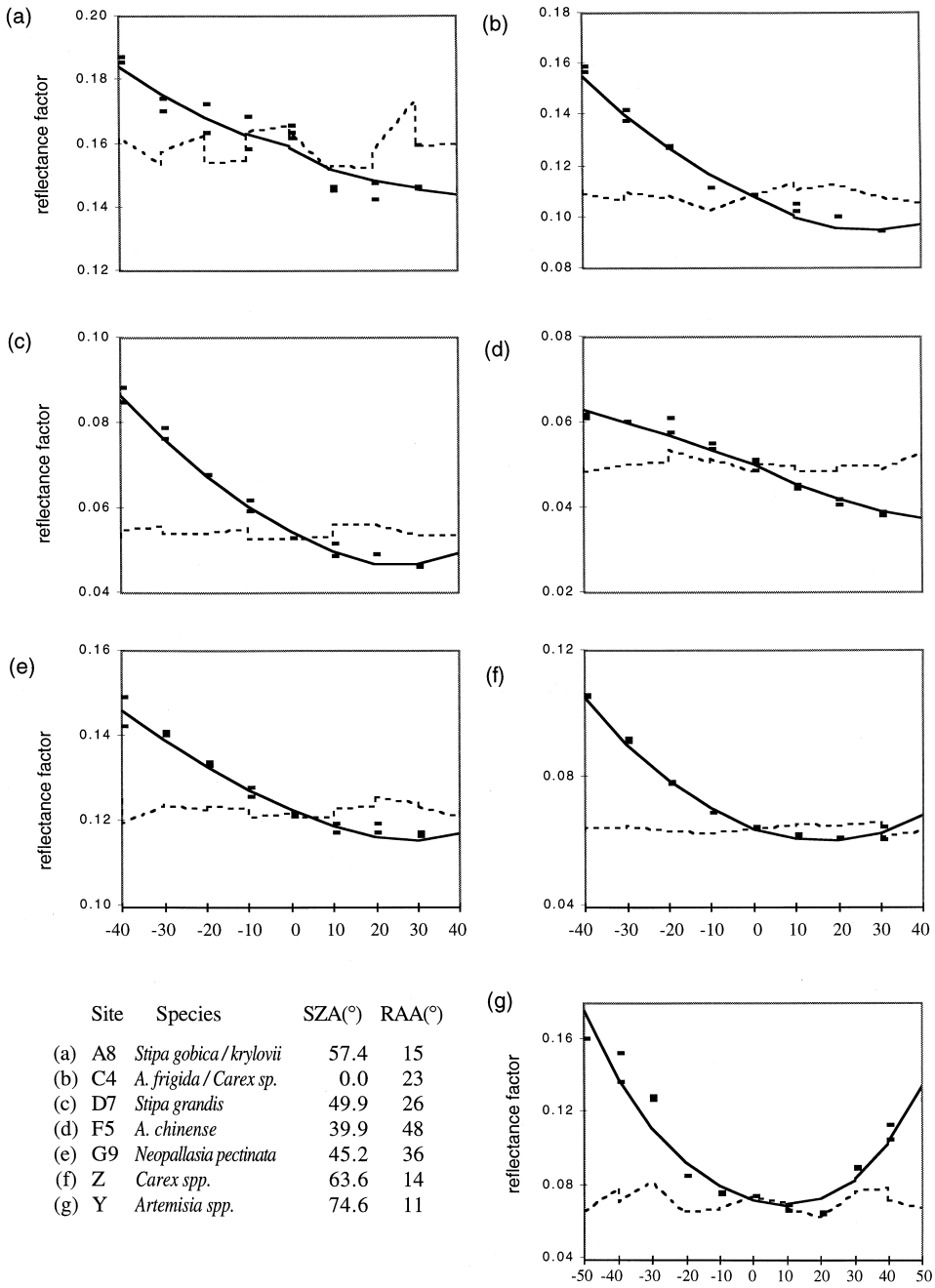

Figure 4. Observed (dots), modeled (solid line), and corrected (dotted line) bidirectional reflectance distributions red channel, Inner Mongolia sites.

Error in Model Fitting

Overall, the model fits are considered very satisfactory. Even though the range of view and illumination angles is not very large and so the model is not highly stressed, residuals from the fit to observations are generally extremely small with RMS errors of between 0.001 and 0.011 (Inner Mongolia) and 0.0002 and 0.006 (Arizona). Using the full three-kernel model, R^2 values range from 0.86 to 0.99 (Inner Mongolia) and 0.91 to 1.00 (Arizona), with only three R^2 values out of 40 lower than 0.90 and 29 greater than 0.95. The model replicated both the NIR and red channel reflectance observations adequately with no important bias with wavelength, and overall the correlation between modeled and measured values is slightly higher in the red (R^2 were 0.994 and 0.997 for Inner Mongolia and Arizona datasets, respectively) than in the NIR (R^2 were 0.983 and 0.992, respectively); see Figure 8. Deviations between the modeled and observed reflectance values do not demonstrate a consistent relationship to view zenith angle. The major cause of large residual values is measurement error, where there is usually a relatively large difference between the individual observations in the pair of readings taken (but note that the absolute divergence in a pair of measurements is =1% reflectance). There may be physical causes for some of these larger residuals; for example, the increased apparent reflectance for site A8 at the +30° view zenith

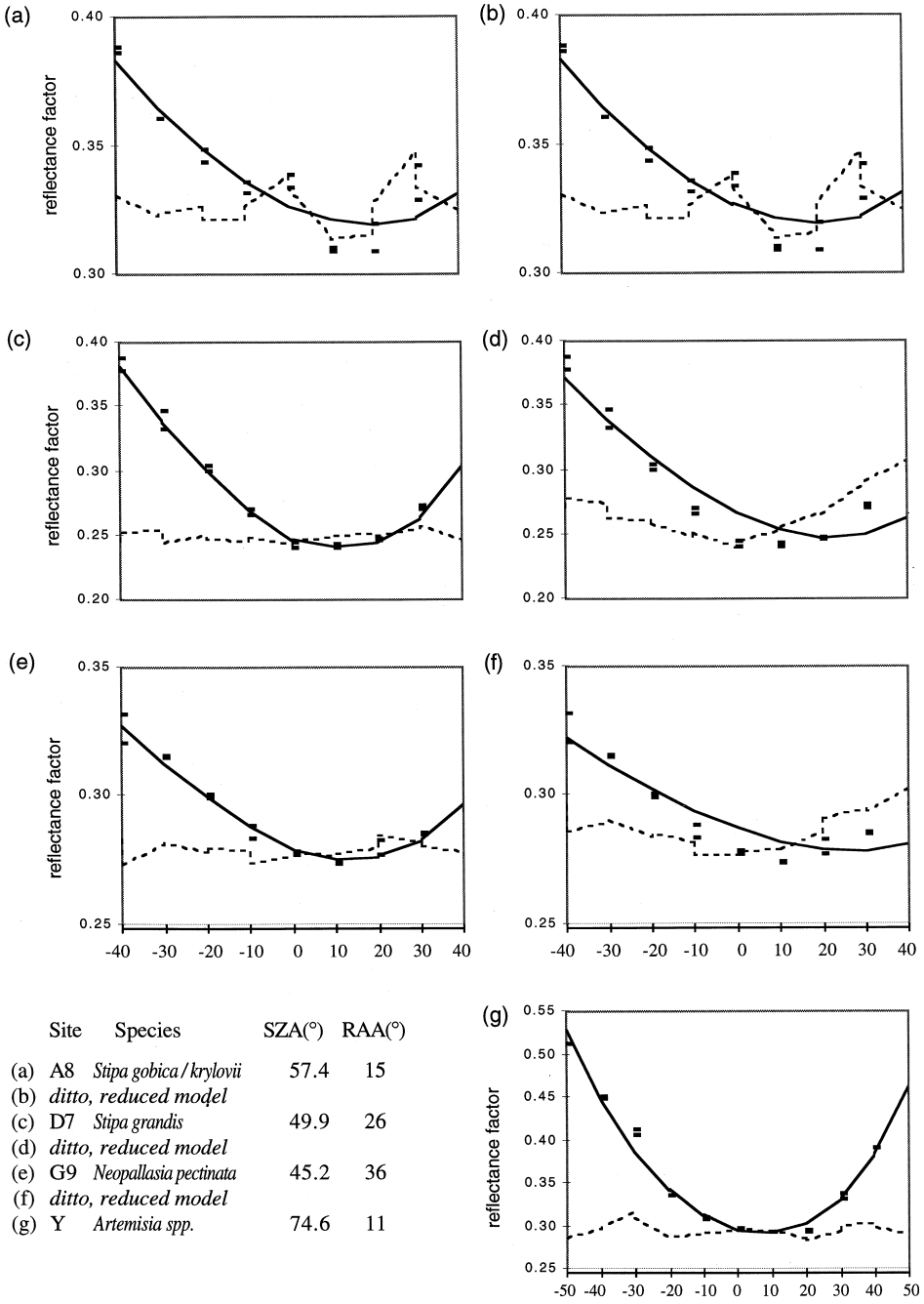

	Site	Species	SZA(°)	RAA(°)
(a)	A8	*Stipa gobica / krylovii*	57.4	15
(b)	*ditto, reduced model*			
(c)	D7	*Stipa grandis*	49.9	26
(d)	*ditto, reduced model*			
(e)	G9	*Neopallasia pectinata*	45.2	36
(f)	*ditto, reduced model*			
(g)	Y	*Artemisia spp.*	74.6	11

Figure 5. Observed (dots), modeled (solid line), and corrected (dotted line) bidirectional reflectance distributions: NIR channel, Inner Mongolia sites. Left side shows results using original model. Right side shows results using reduced model: $R=k_0+k_2f_2$.

may be owing to specular effects since at this time of year the *Stipa krylovii* flower is a light color, rather shiny, and highly curved in shape, and therefore some of the "shine" is likely to be in the sensor's IFOV.

Potential sources of error in the observed reflectance data include pointing the sensor at the wrong place or in the wrong geometry; foreign objects intruding into the sensor IFOV; the IFOV not being large enough to integrate all surface components in sparsely distributed canopies; anisotropy in the spectral reflectance of the halon reference panel; wind [or what is called "nebulosity" by Guyot (1990)]; contamination of the reference panel by windborne debris; inadvertent shadowing of the target or reference panel; and poor illumination conditions. Most of these factors were well controlled in these experiments. For very precise measurement of bidirectional reflectance, it is sometimes considered necessary to effect a correction for the non-Lambertian properties of the reference panel; however, here the assumption is made that the pressed halon panel used has quasi-Lambertian reflectance properties, following published research: Jackson et al. (1987) found that a pressed halon panel exhibited a variation from the mean of 0.2% for incidence angles ranging from 20° to 70° over a series of seven measurements. Research on

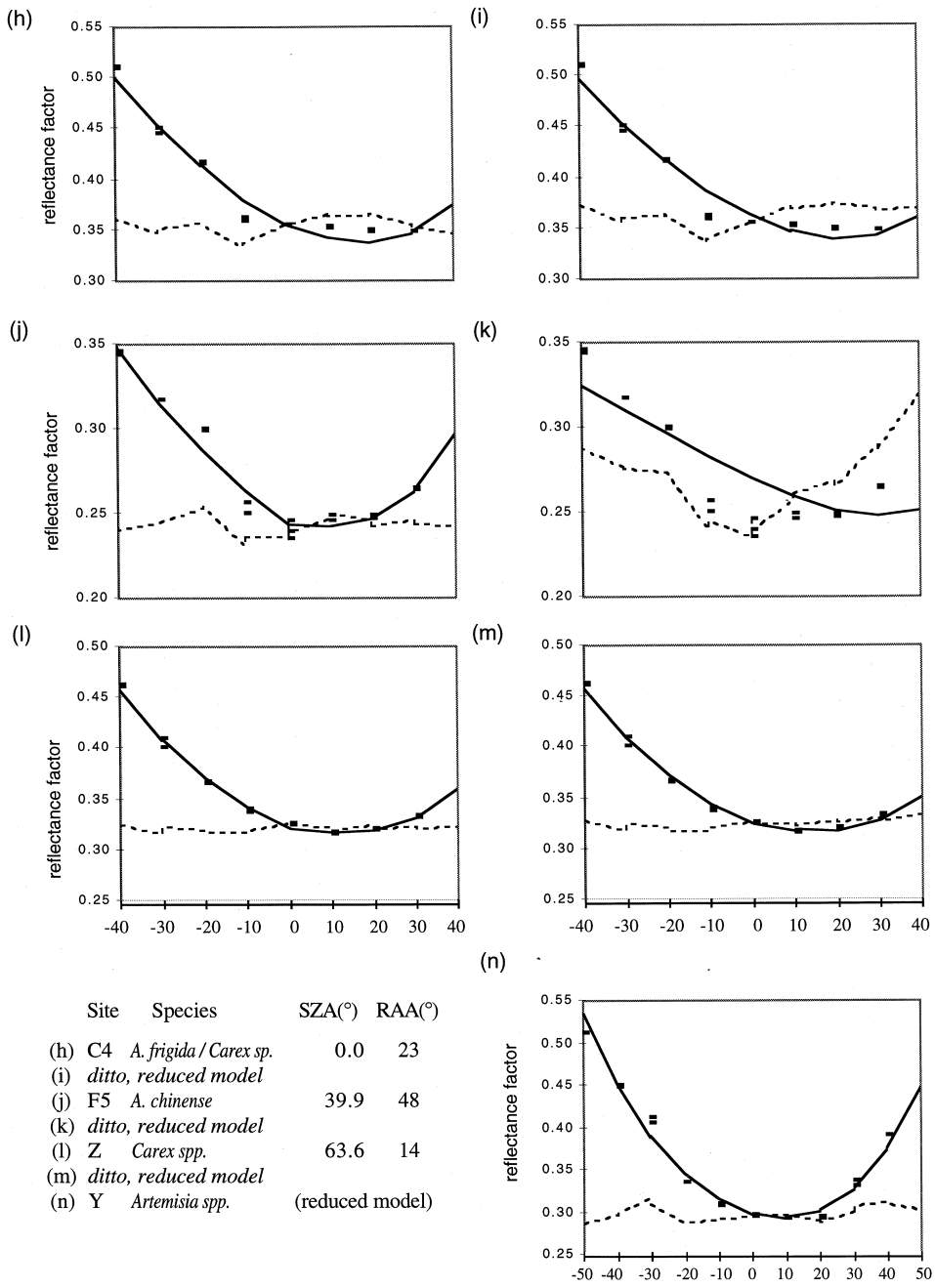

Figure 5. Continued.

optical-grade Spectralon™, a PTFE-based material similar to that used here, shows that at incidence angles up to 60°, variation in the reflectance of the global flux with angle is close to Lambertian (Rollin et al., 1996). These authors also suggest that with such a reference panel it is not necessary to make corrections for the non-Lambertian properties of the panel for solar zenith angles of up to 60° since the deviation from Lambertian over this range is <2% and is likely to be within measurement error. Solar zenith angles reported here exceed 60° in three cases in the Inner Mongolia data set and in one case in the Arizona data set. Note that only one azimuthal string from the latter data set comes close to a hot spot geometry with no reduction in the quality of model fitting in either channel; this is because the hot spot for this surface has a very narrow angular width, which cannot be captured with the 15° IFOV of the radiometer.

Correction for Directional Effects

The corrected or normalized reflectance data are plotted alongside the observed and modeled values in Figures 4 to 7. The intention is to demonstrate the utility of the BRDF model in removing the dependence on view angle in surface reflectance data. The standard deviation of the observed reflectances series in both channels is reduced by more than 60% after normalization in all cases, with

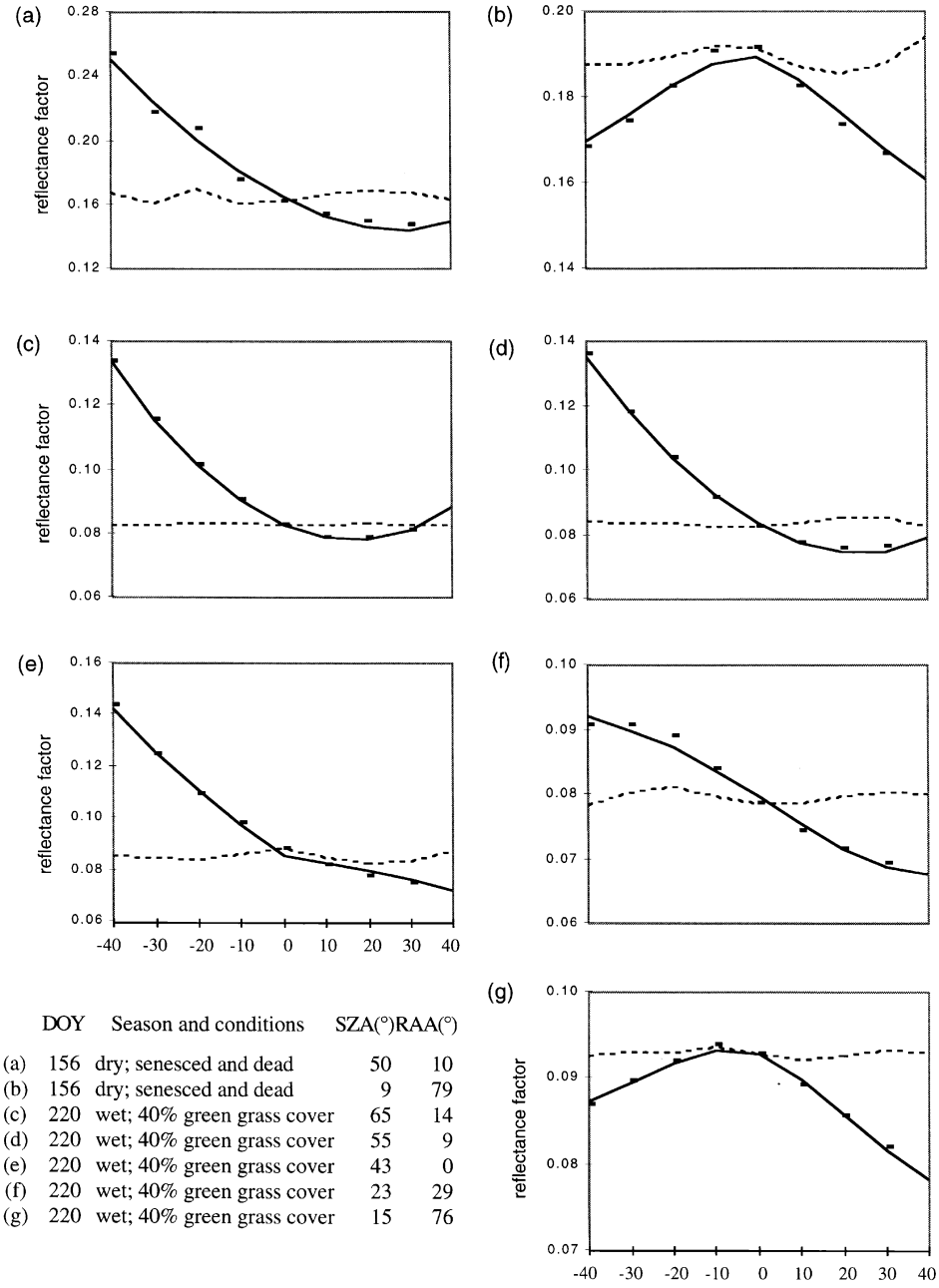

	DOY	Season and conditions	SZA(°)	RAA(°)
(a)	156	dry; senesced and dead	50	10
(b)	156	dry; senesced and dead	9	79
(c)	220	wet; 40% green grass cover	65	14
(d)	220	wet; 40% green grass cover	55	9
(e)	220	wet; 40% green grass cover	43	0
(f)	220	wet; 40% green grass cover	23	29
(g)	220	wet; 40% green grass cover	15	76

Figure 6. Observed (dots), modeled (solid line), and corrected (dotted line) bidirectional reflectance distributions: red channel, Walnut Gulch, Arizona.

much better reductions in most cases. The standard deviation in the normalized reflectances is always≤0.01 reflectance. The correction of the red and NIR channel field-derived reflectance data also provides an opportunity to examine the potential improvement for applications, such as detailed land cover-type classification, which rely on the ability of a classification algorithm to determine class boundaries in feature space. Figure 9b shows the reflectance data for each site in red-NIR space, corrected to nadir viewing with the sun at the mean acquisition angle, together with the uncorrected reflectance data in Figure 9a. This is the optimal geometry for these particular sets of observations (interpolation to the mean view zenith and no extrapolation to unobserved sun zeniths). The distribution of corrected data points for sites belonging to the same grassland types is clearly more favorable for the classification problem; the data points that are clustered in the lower left part of the plot correspond to grassland types, which are rather similar in terms of vegetation cover and species composition: *Stipa grandis*-typical steppe and grazed *A. chinense*-typical steppe. In contrast, the scatter of points in the uncorrected data set means that only the pure *Stipa gobica* desert steppe class (site A2) can be completely isolated with confidence via classification algorithms.

Evaluation of Model Parameters

High correlation coefficients between observed and modeled BRFs do not necessarily mean that the model is able

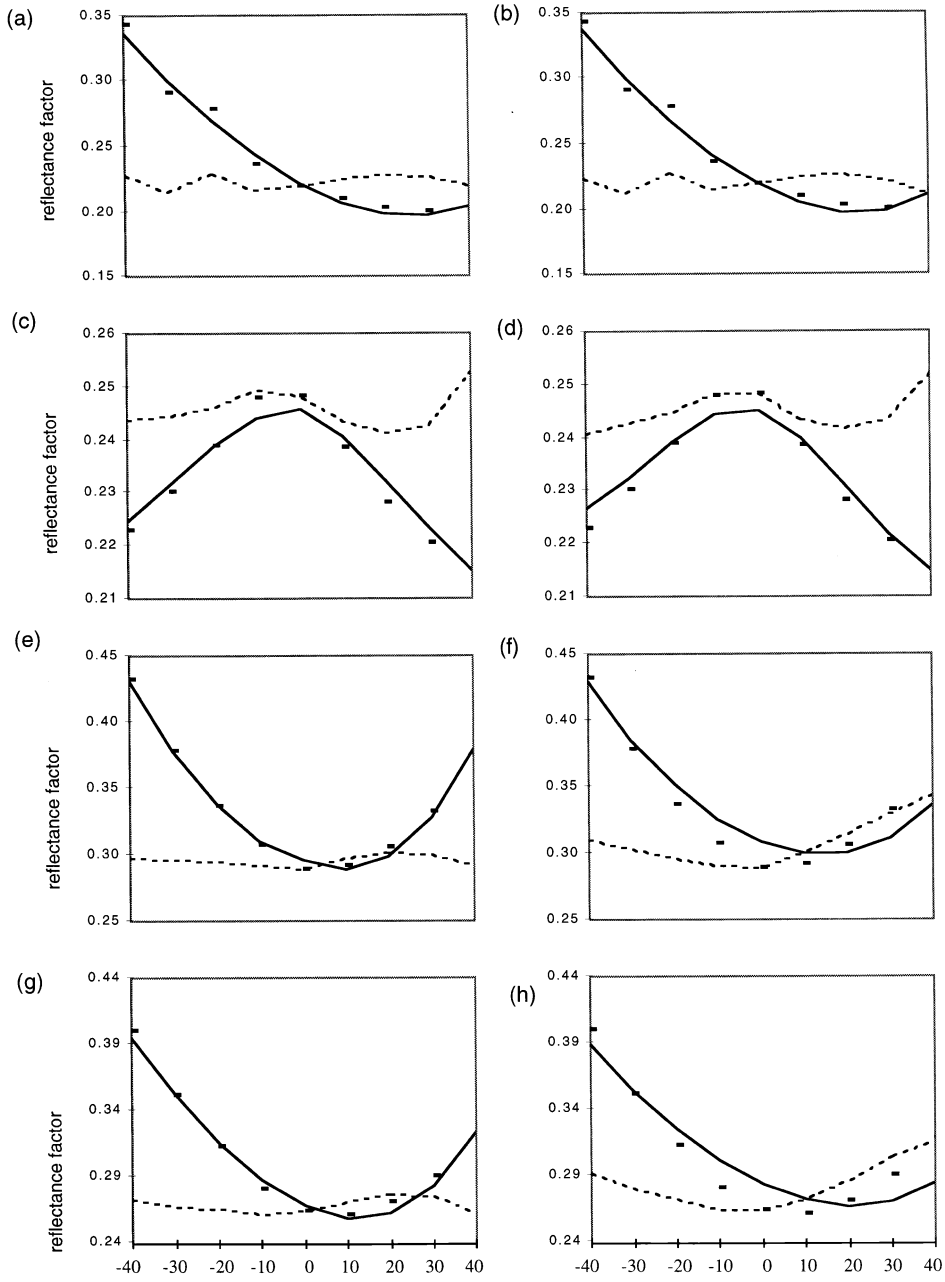

Figure 7. Observed (dots), modeled (solid line), and corrected (dotted line) bidirectional reflectance distributions: NIR channel, Walnut Gulch, Arizona. Left side shows results using original model. Right side shows results using $R=k_0+k_2f_2$.

to explain the interactions of radiation with the canopy-soil complex. It is necessary to determine whether the model kernels behave in the expected manner when the retrieved surface parameters (kernel weights) are applied to them, remembering that surface scattering kernels are generally formulated to deplete reflectance, while volume scattering kernels generally enhance reflectance (Fig. 3). The k_0 parameter is the modeled reflectance at nadir viewing with the overhead sun, and in all cases it is shown to be reasonable, with values corresponding to known surface conditions: for both the Inner Mongolia and Arizona data sets there is a decline in the modeled isotropic reflectance in both wavelength regions from sparsely vegetated surfaces to higher-cover sites (Inner Mongolia), and from DOY 156 to DOY 220 as the vegetation changes from senesced/dead to green (Arizona). The k_1 parameter should provide an estimate of the magnitude of geometric and shadowing effects in total reflectance, and in the red wavelengths it behaves in the expected manner, being consistently positive with only one exception (in the DOY 156 data set where it is very close to zero). For the Inner Mongolia data set, red channel k_1 values generally appear to be related to green vegetation cover, and k_1 generally increases with sparseness. Large geometric and shadowing effects would be expected in the low-cover desert steppe sites since in all three sites the vegetation is clumped on very bright soil backgrounds. However, no consistent relationship is seen in the Arizona model fits.

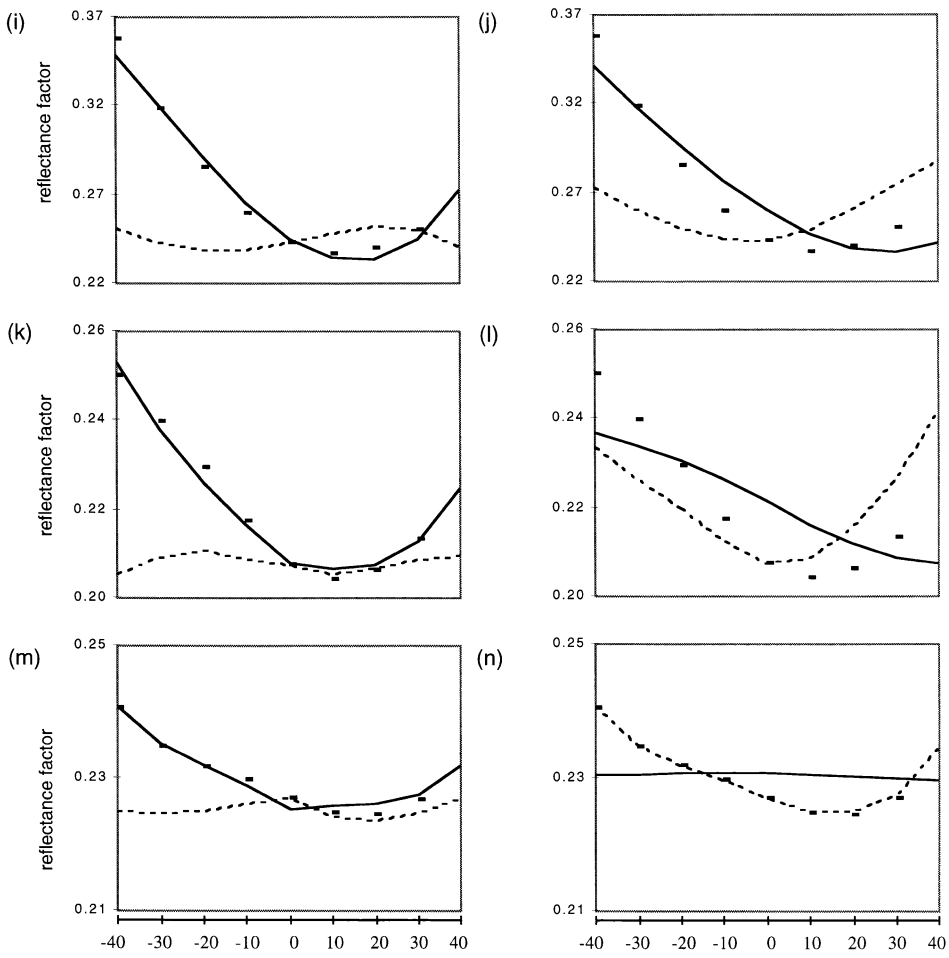

	DOY	Season and conditions	SZA(°)	RAA(°)		
(a)	156	dry; senesced and dead	50	10	(b)	as (a) with reduced model
(c)	156	dry; senesced and dead	9	79	(d)	as (c) with reduced model
(e)	220	wet; 40% green grass cover	65	14	(f)	as (e) with reduced model
(g)	220	wet; 40% green grass cover	55	9	(h)	as (g) with reduced model
(i)	220	wet; 40% green grass cover	43	0	(j)	as (i) with reduced model
(k)	220	wet; 40% green grass cover	23	29	(l)	as (k) with reduced model
(m)	220	wet; 40% green grass cover	15	76	(n)	as (m) with reduced model

Figure 7. Continued.

In the NIR channel negative and unphysical k_1 values were obtained in all but two cases in the Inner Mongolia model fits and for all the Arizona DOY 220 model fits; the geometric and volume kernels are both contributing to reflectance in a similar manner. Other workers have found that the model fits sometimes provide very small or negative values and have set this parameter to zero. In both Roujean et al. (1992a) and Wu et al. (1995) low or negative k_1 were obtained with forest-cover and cropland land-cover types. Negative parameter values were also obtained by Roujean et al. (1997) with airborne POLDER data over the HAPEX-Sahel Central-West supersite (Niger) and by Takemata et al. (1999) with satellite-level POLDER data over bare soil, desert, grassland, and forest sites in Mongolia. These values are usually explained as a result of the small volume of and errors in the data sets and of mathematical anomalies in model fitting. In the cases examined here, there appears to be some relationship between the absolute magnitude of the parameter and green vegetation amount and structure: in the Inner Mongolia cases there is a higher absolute magnitude in k_1 with increasing canopy height and density, with the largest absolute values obtained for sites D7 (*Stipa grandis* typical steppe at 1-m maximum height), D8 (similar), and F5 (fairly lush *Aneurolipideum chinense*-typical steppe); while in the Arizona model fits k_1 is consistently much larger in absolute terms for the DOY 220 cases (40% cover green gramma) than for the DOY 156 cases (senesced/dead vegetation). In the Inner Mongolia cases where positive (albeit very small) k_1 are obtained, vegetation is sparse. In previous evaluations of the model low or negative k_1 are set to zero, thereby reducing the model as seen in Eq. (6):

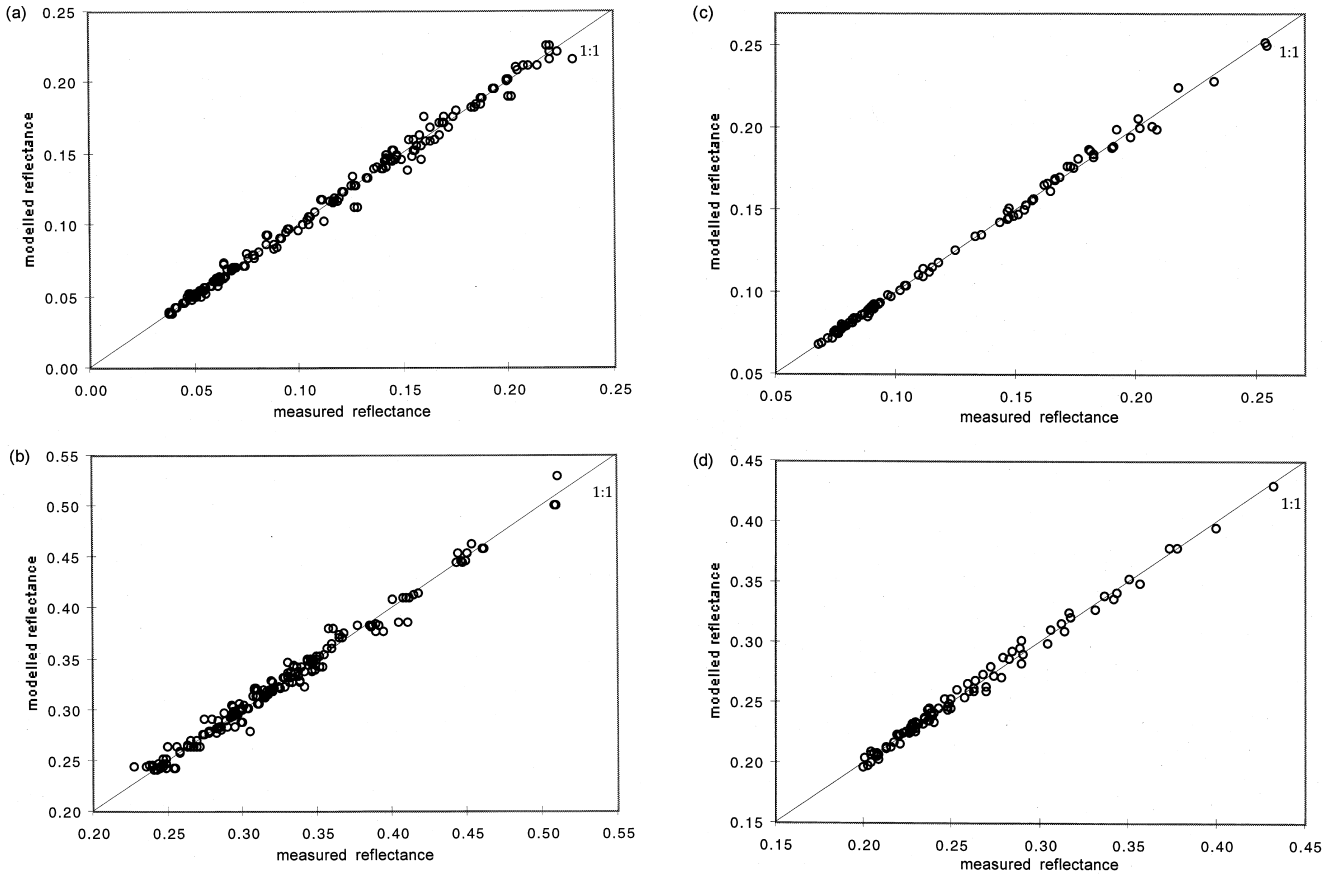

Figure 8. Modeled vs. measured reflectance: (a) red channel (Xilingol, Inner Mongolia), (b) NIR channel (Xilingol, Inner Mongolia), (c) red channel (Walnut Gulch, Arizona), and (d) NIR channel (Walnut Gulch, Arizona).

$$R(\theta_s,\theta_v,\varphi)=k_0+k_2\ f_2(\theta_s,\theta_v,\varphi) \qquad (6)$$

that is, accounting only for an isotropic component and a volume scattering component. When this reduced model is applied to the NIR reflectance factor data, the model fits remain very good for cases where there is low cover, greenness, or canopy height, but become poor for the cases where cover is relatively high, the leaves are greener, or the canopy is taller. The results of the NIR data fits to the reduced model are shown in Tables 2 and 3 and Figures 5 and 7 (right-hand column). There is one exception to this behavior for site Y, and this may be a result of the very high solar zenith angle (75°). Canopy height may be an important factor in this phenomenon since where cover is high but canopy height is low (site Z, 74% cover grazed lowland *Carex* sp. pasture with a maximum height of 8 cm), R^2 remains high with the reduced model (0.99).

Note that although the problem is manifested through unreasonable k_1 values, the underlying problem is not necessarily the geometric/shadowing function but could equally well be connected with the volume scattering kernel. To investigate the anomaly, it is helpful to examine the relative contributions made by the weighted model kernels to the anisotropic component of reflectance (Fig. 10). In general NIR $k_1 f_1$ either reduces reflectance or makes virtually no contribution in the sparse and dry season cases, but enhances reflectance anisotropically in the more-vegetated and wet season cases. The kernel is clearly not accounting for geometric-optical effects as intended, but may be inadvertently accounting for other physical phenomena. The contribution is positive and anisotropic, increasing with view zenith angle from the backscattering to the forward-scattering direction; low-order multiple scattering is a possible cause.

The suggestion of a problem with a "dense" volume scattering kernel over semiarid targets is supported by other recent studies that show that the isotropic-RossThin-LiSparseMODIS combination performs better than other kernel combinations (Lewis et al., 1998; Chopping, 1998a). There are two approximations made in the derivation of this kernel that might explain its inadequacy here: (1) the approximation made in taking the optically thick case and (2) the single scattering approximation. In determining which of the two is more important, the following arguments may be pursued:

1. Taking the optically thin case is preferable. According to Roujean et al. (1992a), the approximation made in taking the optically thick case is rather gross for situations where LAI is $\leqslant 1$, as here, with quite important relative errors in the most unfavorable configurations. In both Inner

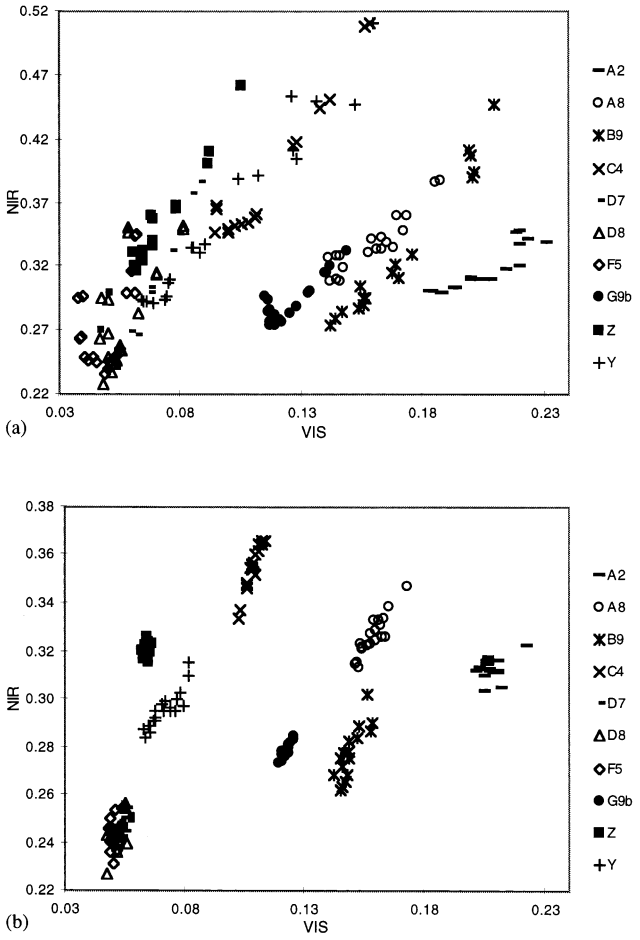

Figure 9. Off-nadir field radiometry (a) uncorrected for BRDF (b) corrected for BRDF to nadir view zenith and mean solar zenith angle. VIS=red channel.

Mongolia and Arizona fits the negatively weighted Roujean f_1 function is used to increment reflectance in the forward-scattering direction; a steeper increase in the contribution of the weighted volume scattering kernel to reflectance in this direction is therefore required to model the observed reflectance using only positive (physical) parameter values. Concurrent studies show that this steeper shape is provided by a kernel derived with the optically thin approximation: both a Roujean f_1-Ross-Thin and a LiSparse-RossThin model provide positive NIR k_1 values, and the geometric-optical parameter decreases with increasing LAI for both red and NIR inversions, as it should (Chopping, 1998a, Chopping, 1998b).

2. The single scattering approximation is inadequate. Although the LAI of the grassland types under consideration is generally <1, the single scattering approximation may also contribute to the requirement for a steeper volume scattering kernel shape. This may be so because such a requirement is only seen in the NIR wavelengths where the single scattering approximation is less likely to be valid; in short, there is likely to be residual anisotropy from multiple scattering in sparse canopies. This is reasonable because it is known that grass leaves have a lower reflectance than transmittance in the NIR, unlike the leaves of crops or trees (Blad, 1988, cited in Wu et al., 1995), and because $k_1 f_1$ enhances reflectance in the backscattering direction as well as the forward-scattering direction. Several studies have shown that multiple scattering is not always isotropic (Li et al., 1994; Schaaf, et al., 1994), although it has also been demonstrated that the additional interactions due to successive scattering orders have a bidirectional signal in which amplitudes decreases sharply as the scattering order increases (Rondeaux, 1990). In semiarid grasslands the order of scattering is likely to be fairly low since the canopies are relatively sparse, soils are bright, and LAI is low; it therefore appears that the single scattering approximation made in the derivation of the volume scattering kernel may not be valid in the NIR wavelengths for semiarid grasslands. This suggestion is supported by Hu et al. (1997), who found that a weak correlation (R^2= 0.56) was obtained when fitting the variants of the AMBRALS model to NIR airborne POLDER observations over grassland [although they attribute this to registration errors, these errors would also have affected the red channel fit where the correlation was somewhat better (R^2=0.71)].

The k_2 parameter should provide an estimate of the contribution of volume scattering and is theoretically a function of facet spectral reflectance and facet area index. Values are consistently positive and larger in the NIR than in the red channel, and this is to be expected since there is much lower absorption of NIR wavelength radiation by either vegetation or soils and higher transmittance through than reflectance from grass leaves, as noted above. In the Inner Mongolia model fitting, the NIR channel k_2 values appear to be qualitatively related to vegetation cover and LAI, with the highest values for sites F5, D7, D8, and B9 (Fig. 11). Similarly, for the Arizona model fits higher values are obtained for the wet season than for the dry season as expected, although this is not completely consistent. Red channel k_2 values do not appear to be highly correlated to vegetation cover or LAI in the Inner Mongolia cases but are consistently higher for the dry season than wet season in the Arizona cases. For both data sets, they are generally in or close to the range expected (0.1 to 0.5 for leaf facets and 0.2 to 0.4 for soil facets) but are somewhat higher than that found by Roujean et al. (1992a) for a steppe with 18% vegetation cover (0.06).

According to the model derivation the k_1 parameter should be related to the size, shape, and spacing of protru-

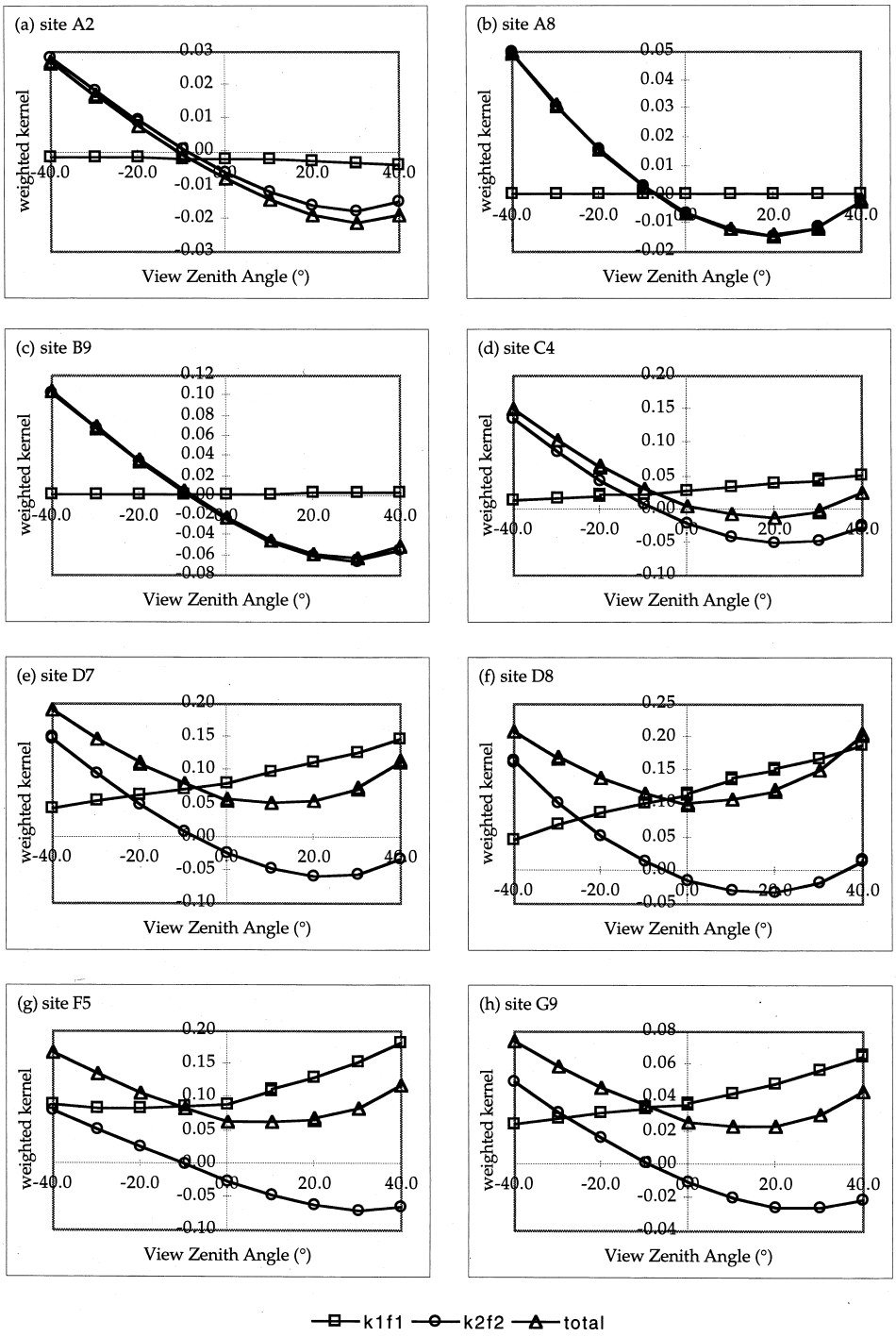

Figure 10. Contributions of weighted kernels to anisotropy in NIR reflectance, (a–h) Xilingol sites, Inner Mongolia; (i–p) Walnut Gulch sites, Arizona.

sions, and the k_2 parameter should be related to LAI. Wu et al. (1995) made the assumption that, to the first approximation, the physical structure and optical properties of canopies are land cover-type specific and found that for the AVHRR data they used, it was possible to retrieve strong relationships between the k_0 parameter, the k_1/k_0, and k_2/k_0 anisotropy factors and NDVI within each land cover type. However, the approximations made in the derivation of the model and the retrieval of negative values in the NIR mean that a direct inverse interpretation of the anisotropic parameters is problematic. Here, the strongest relationships are seen between the red channel geometric-optical parameter and both fraction of cover and LAI, while a strong relationship is seen between the NIR channel geometric-optical parameter and LAI. The volume scattering parameter demonstrates very weak relationships to both measures; see Table 4 and Figure 11. Thus, the concluding remark of Roujean et al. (1992a) to the effect that it is

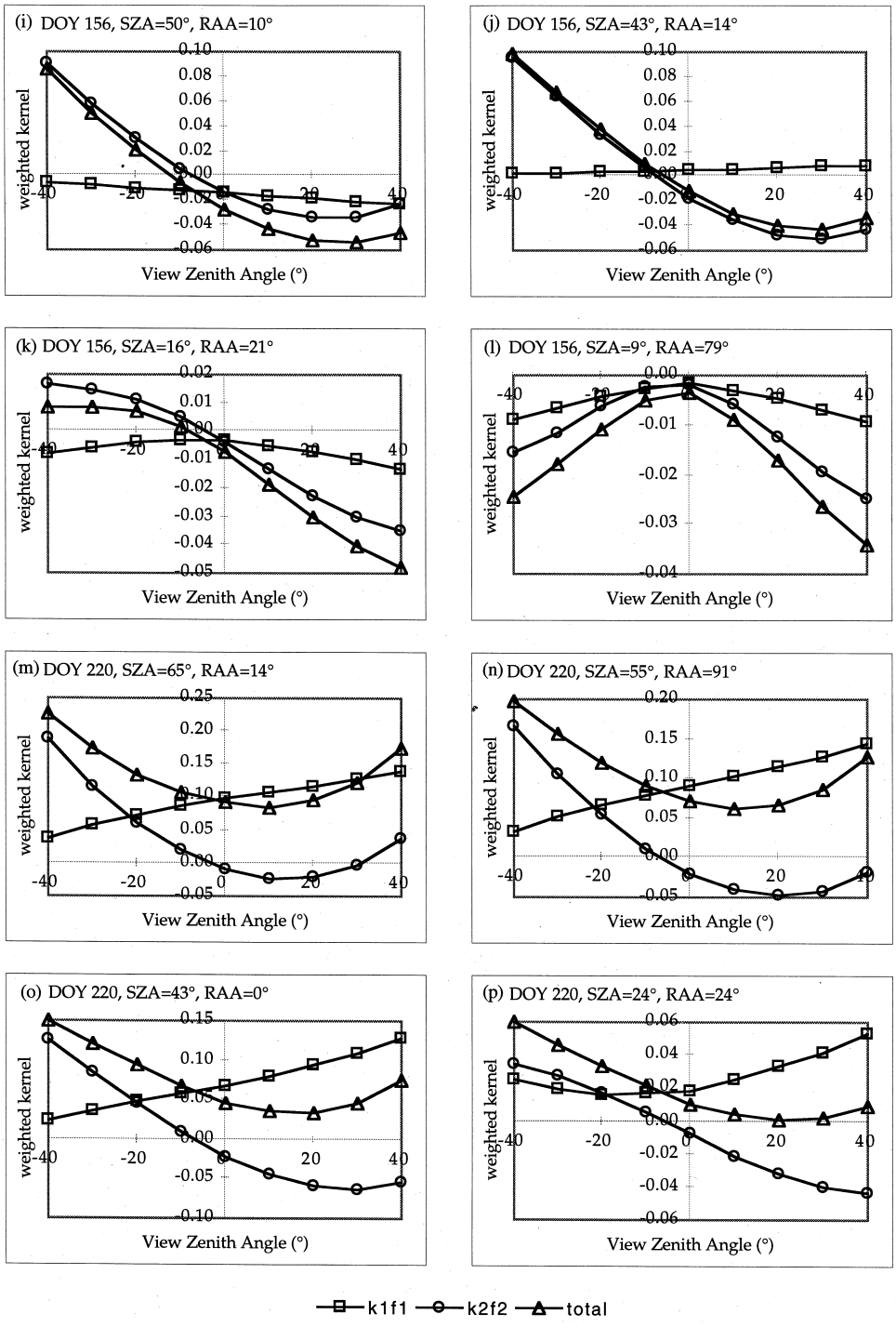

Figure 10. Continued.

not possible to ensure a physical interpretation of these parameters does apply here, although there is clearly additional, nonspectral information present in kernel weights.

Model Sensitivity

An important characteristic of any model is the degree of sensitivity to inputs, in this case the number and angular distribution of observations. This is particularly important for satellite remote sensing applications since in the solar reflective wavelengths cloud cover can reduce both the number and angular range of observations substantially, even if the orbital and scanning characteristics of a particular platform and sensor offer a high temporal resolution (for example, one or two observations per location per day). To assess the stability of the model with various small numbers of samples (N) decreasing from the maximum available in the two data sets used, the model fitting procedure was run again four additional times to provide new

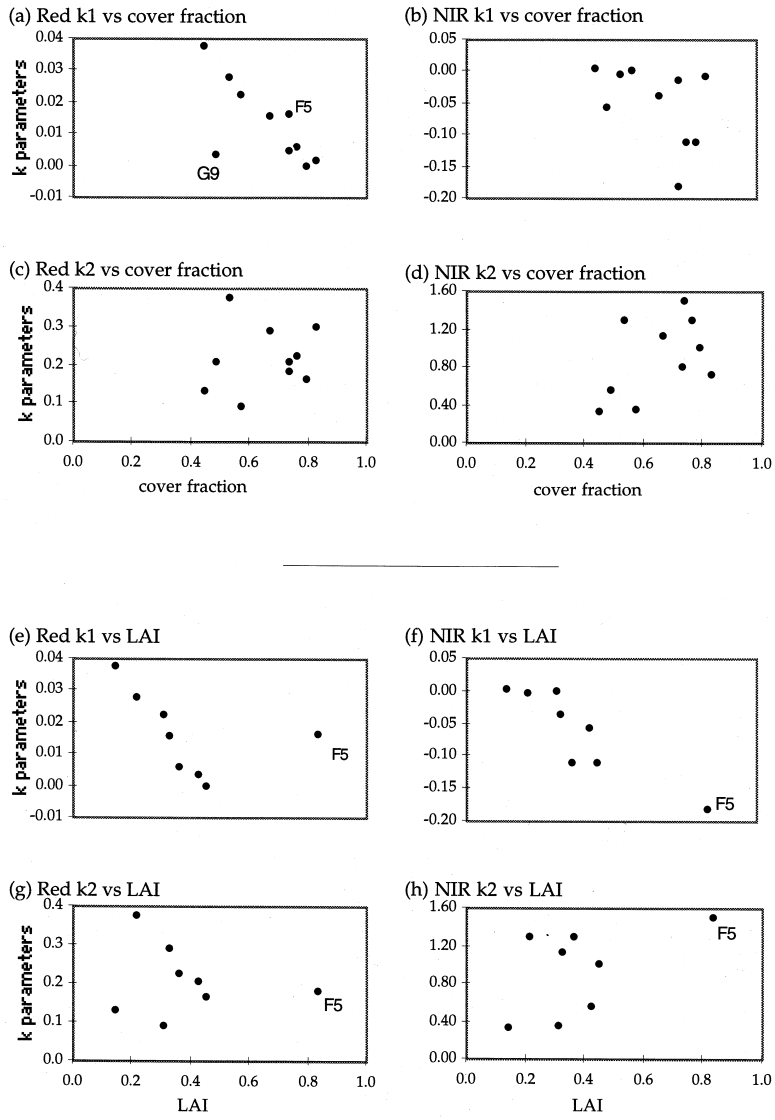

Figure 11. Anisotropic parameters vs. fraction of cover and LAI. Cover calculated from multiple 4-m nadir photographs with shadow allocated to soil or vegetation classes on the basis of the vegetation:soil ratio. LAI plots exclude sites Z and Y (Huhehaote). Note: Y axis scales differ.

sets of outputs. The number of observations was reduced from the original number of between 16 to 22 to 13, 9, 7, and 5 for the Inner Mongolia fits and from 9 to 8, 7, 6, and 5 for the Arizona fits. Reduction in N was achieved by weeding the original data sets, first by removing duplicate observations (i.e., readings taken at the same view angle) and then by removing observations at intermediate angles (no account was taken of the significance of individual observations or the residuals provided by each observation). To test model sensitivity for cases where the angular sampling is limited to either the backscattering or the forward-scattering directions, model fitting was effected with two further data sets derived from the Inner Mongolia radiometry: one where all the observations in the backscattering direction are removed, and one where all the observations in the forward-scattering direction are removed (with the nadir observations retained in both cases).

The results of the analysis for varying numbers of observations are given in Figures 12 to 14. It is inappropriate to use the standard coefficient of determination since

Table 4. Strength of Relationships (R^2) between Model and Effective Biophysical Parameters

	Red k_0	*Red* k_1	*Red* k_2	*NIR* k_0	*NIR* k_1	*NIR* k_2
Cover[a]	0.81	0.51	0.02	0.28	0.21	0.23
LAI[b]	0.55	0.22	0.02	0.45	0.81	0.27
Weight[b]	0.70	0.39	0.02	0.66	0.58	0.36

[a] 4-m photographs with shadow allocated on the basis of the soil-vegetation ratio.
[b] Excluding sites Y and Z; weight is fresh weight.

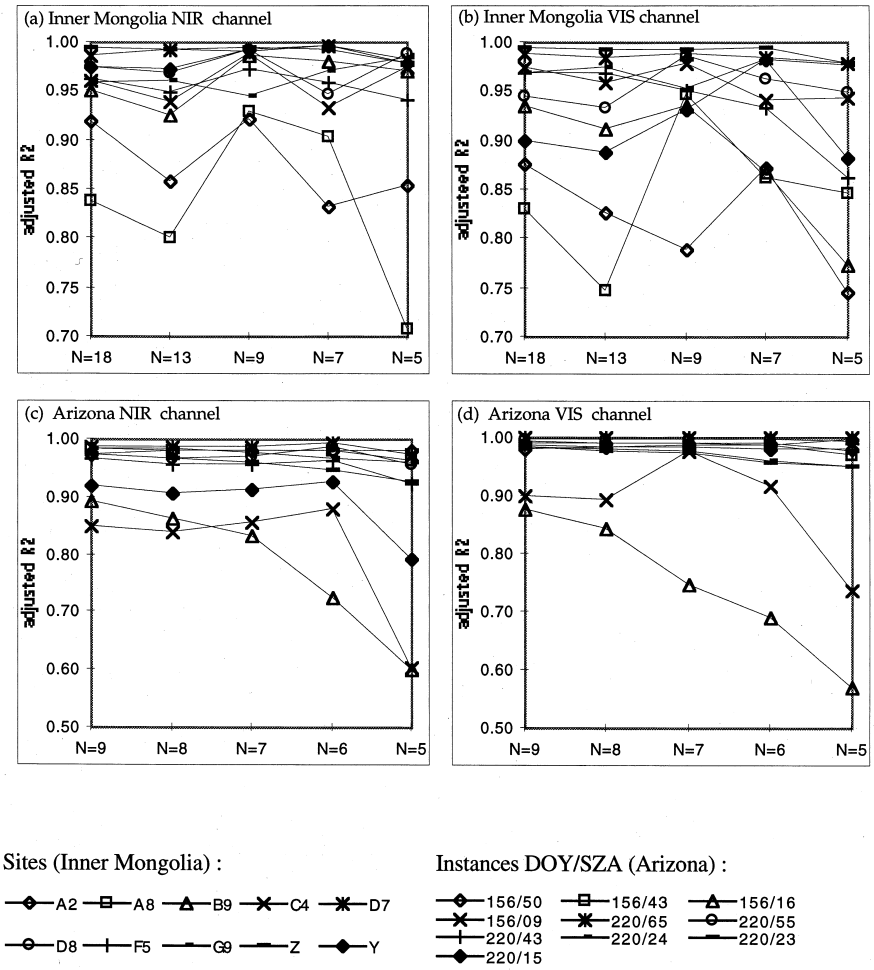

Figure 12. Sensitivity of model fit (adjusted R^2) to number of observations.

the number of observations varies, so the adjusted R^2 is used (Kmenta, 1986, p. 411). Figure 12 shows that the model fits generally remain very good with small numbers of observation well distributed in the view zenith domain, with adjusted R^2>0.95 in the majority of cases, for both red and NIR channel fits. In general, there is a decline in correlation with decreasing N, although the reduction in fitting accuracy is not a linear function of N. For those model fits that show a lower adjusted R^2, the higher degree of variation with reductions in N is similar in both red and NIR channels and, more importantly, occurs mainly for sparse steppe (sites A2 and A8, Inner Mongolia) and dry season (DOY 156, Arizona) model fits.

The results of the analysis for varying the azimuthal distribution are given in Tables 5 to 8. The k_0 parameter values retrieved via sampling in the forward-scattering direction differ only slightly from those obtained using observations distributed in both directions in both channels [usually within 0.01 or 0.02 (reflectance)], while the k_1 parameter values differ by a larger margin, and the k_2 parameter is far less stable (Tables 5 and 6). In contrast, all parameters retrieved via sampling in the backscattering direction differ importantly from those obtained using observations distributed in both directions in both channels. An examination of the weights of determination [a statistical indication of expected error in parameters or on interpolation or extrapolation under specific angular sampling conditions; see Lewis and Wanner (1996)] shows that the k_0 parameter is most stable, followed by the k_1 and k_2 parameters, respectively, with large error expected in the latter (Table 7). The weight of determination is lower for all site Y parameters (where view zeniths were ±50°) and higher for the Arizona parameters (where the sampling is far from the principal plane). Note that the k_0 parameter represents an extrapolation to nadir viewing with the sun at zenith. An examination of the weights of determination for modeled reflectance for nadir viewing with the sun at the mean zenith of the observations shows that in relation to sampling in both directions, noise inflation is somewhat higher for forward-scattering but is much higher for backscattering (Table 8). There is no noise inflation for the distributions with sampling in both directions; the weight of determination is below unity in all cases.

Model parameters are thus very stable with reductions in the number of observations, even with the minimum of five, as long as the angular distribution is adequate (Figs. 13 and 14). For the cases where observations in both backscattering and forward-scattering directions are used, the k_0

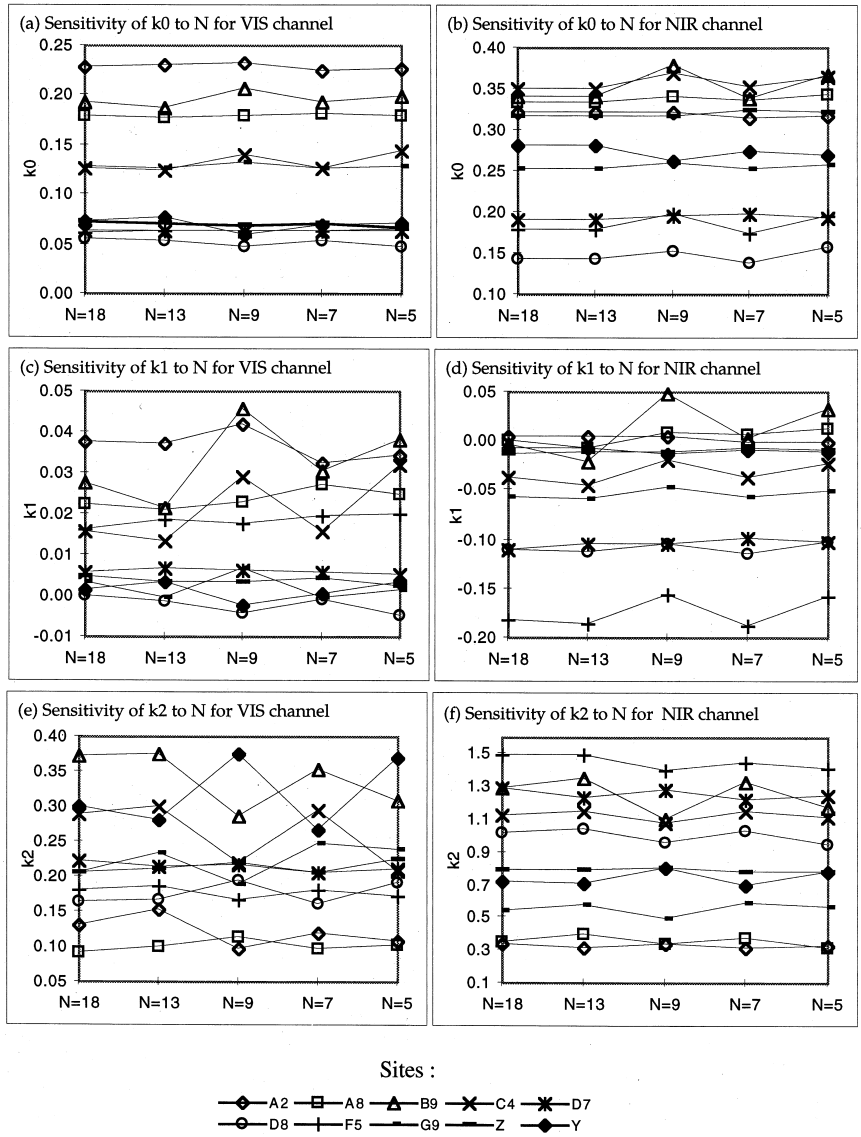

Figure 13. Sensitivity of model parameters to varying numbers of observations for Inner Mongolian sites.

parameter is extremely stable, with a standard deviation of less than 2% reflectance and less than 1% in 18 of 20 cases for Inner Mongolia, and by less than 0.4% in 18 of 20 cases for Arizona. The anisotropic surface parameters were found to be less stable with respect to N, with the k_2 parameter consistently having far more noise than the k_1 parameter. Where the angular sampling is in only one half-space, the stability of modeled reflectance at nadir viewing with the sun at the mean zenith of the observations is severely compromised if sampling is only in the backscattering direction, with a lesser impact if sampling is only in the forward-scattering direction.

CONCLUSIONS

This study has demonstrated that the Roujean model is able to describe with good accuracy the variations in surface reflectance from semiarid grassland canopies of differing densities and architectures with changing view and illumination geometries, within the angular limits of the data sets used. Modeled reflectance values have been shown to be close to observed values for two independent semiarid grassland bidirectional reflectance factor data sets, enabling normalization of observed surface reflectances to a preferred geometry and providing a means of achieving an adequate reduction in directional dependency in surface reflectance series. This was the stated aim of Roujean et al. (1992a) in deriving the model.

The retrieval of negative surface parameters is sometimes regarded as the result of mathematical anomalies in model fitting (Roujean et al., 1992a; Wu et al., 1995; Wanner et al., 1995; Roujean et al., 1997; Takemata et al., 1999). In this study the possible reasons for these artifacts were explored, and it was found that while the positive contribution to the anisotropic component of reflectance resulting from the negatively weighted f_1 kernel may be

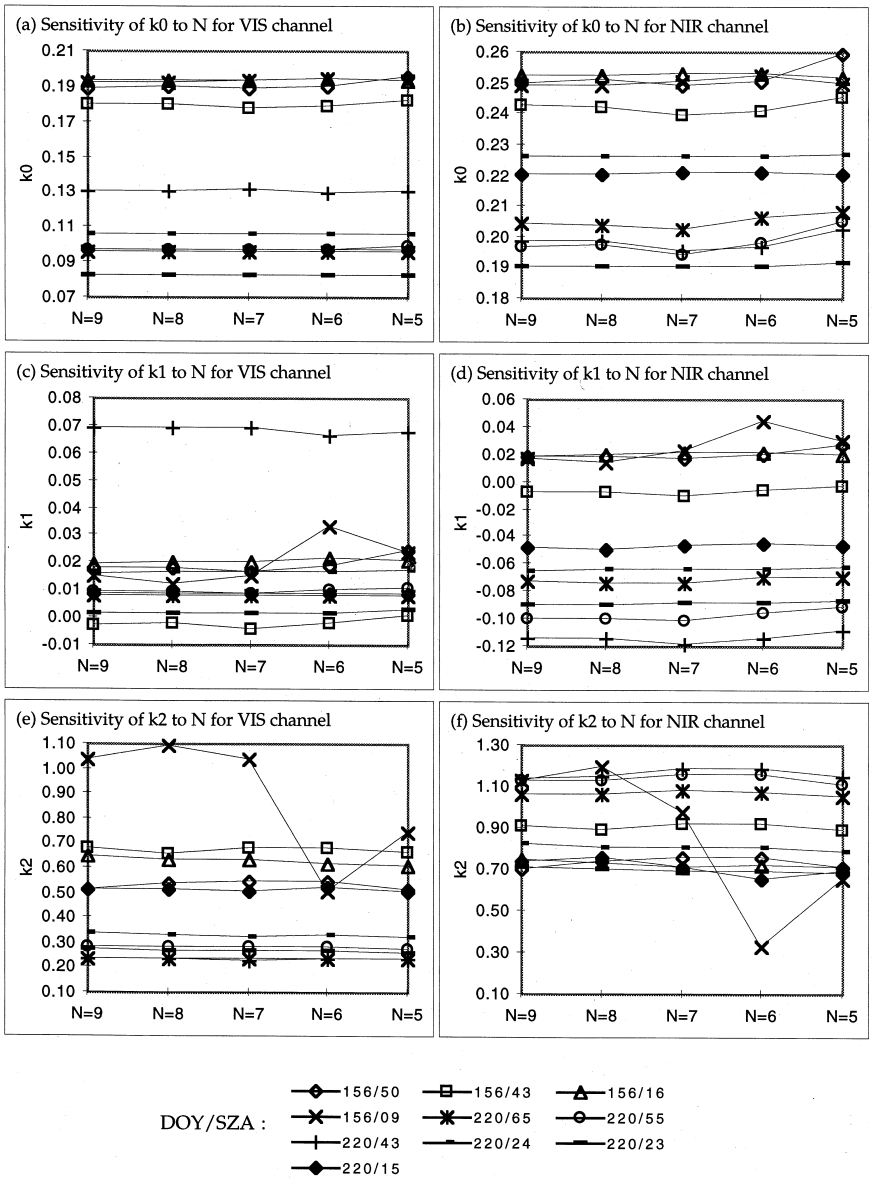

Figure 14. Sensitivity of model parameters to varying numbers of observations for Arizona Sites.

omitted for very low LAI and sparse canopies, it is necessary to obtain good fits to NIR observations for relatively high LAI and erectophile grassland canopies. Thus, adopting a unique set of kernels to physically model light scattering in both the red and NIR wavelength may not be feasible since the interactions are quite different. While it is not possible to determine whether the assumption of an optically thick or optically thin surface is more valid in the red wavelengths, there is a strong case for considering that the single scattering approximation is at the root of the problems in modeling NIR wavelength interactions. Changing to an assumption of an optically thin surface may only lead to positive parameter retrievals as a result of inadvertent modeling of residual anisotropy arising from low-order multiple scattering, although this is not proven here. In addition, the geometric-optic kernel may also be inadequate in the NIR region since it may not be reasonable to consider grass leaves as opaque protrusions. The implication is that the complex interactions of NIR radiation with grassland canopies are not explained exactly by the model. Despite this it is able to describe the shapes of the NIR BRFs for all sites well and may therefore be effective in BRDF correction, which has been shown to have a very important impact on data quality.

Interpretation of the model parameters in terms of biophysical parameters is problematic, partly for the reasons given above and partly because there are insufficient data with which to establish relationships. Strong correlations were found between the red channel isotropic parameter and cover fraction, LAI, and fresh weight; the red channel k_1 and cover fraction; the NIR channel isotropic parameter and fresh weight; and the NIR channel k_1 parameter and LAI and fresh weight. The sensitivity analysis shows that the model is remarkably robust with respect to

Table 5. Model Sensitivity to Azimuthal Sampling, Inner Mongolia Sites

	Red Channel Parameters									*NIR Channel Parameters*								
	k_0 *(iso)*			k_1 *(geo)*			k_2 *(vol)*			k_0 *(iso)*			k_1 *(geo)*			k_2 *(vol)*		
Site	*All*	*Back*	*Fwd*	*All*	*Back*	*Fwd*	*All*	*Back*	*Fwd*	*All*	*Back*	*Fwd*	*All*	*Back*	*Fwd*	*All*	*Back*	*Fwd*
A2	0.23	0.33	0.22	0.04	0.25	0.03	0.13	−0.16	0.17	0.32	0.50	0.32	0.00	0.37	0.01	0.34	−0.06	0.16
A9	0.18	0.37	0.19	0.02	0.28	0.03	0.09	−0.64	0.22	0.33	0.67	0.35	0.00	0.44	0.01	0.35	−0.93	0.52
B9	0.19	0.37	0.19	0.03	0.38	0.04	0.37	−0.08	0.11	0.34	0.54	0.34	−0.00	0.41	0.05	1.30	0.86	0.18
C4	0.13	0.01	0.13	0.02	−0.16	0.02	0.29	0.75	0.13	0.35	0.02	0.36	−0.04	−0.52	−0.01	1.12	2.44	0.63
D7	0.06	0.10	0.06	0.01	0.06	0.01	0.22	0.09	0.14	0.19	0.25	0.18	−0.11	−0.01	−0.11	1.29	1.08	0.89
D8	0.05	0.06	0.06	0.00	0.01	0.00	0.16	0.14	0.22	0.14	0.43	0.14	−0.11	0.18	−0.11	1.01	−0.04	1.04
F5	0.06	0.09	0.06	0.02	0.08	0.01	0.18	0.16	0.30	0.18	0.30	0.18	−0.18	0.07	−0.16	1.50	1.52	1.13
G9	0.13	0.21	0.13	0.00	0.14	0.01	0.21	−0.05	0.06	0.25	0.43	0.25	−0.06	0.24	−0.05	0.55	−0.01	0.33
Z	0.07	0.03	0.07	0.00	−0.03	0.00	0.20	0.35	0.18	0.32	0.07	0.33	−0.01	−0.23	−0.00	0.79	1.63	0.81
Y	0.07	−0.22	0.07	0.00	−0.17	−0.00	0.30	1.05	0.28	0.28	−0.01	0.27	−0.01	−0.18	−0.01	0.72	1.46	0.71

All=both half-spaces; Back=backscattering only; Fwd=forward-scattering only.

Table 6. Model Sensitivity to Azimuthal Sampling, Arizona Sites

	Red Channel Parameters									*NIR Channel Parameters*								
	k_0 *(iso)*			k_1 *(geo)*			k_2 *(vol)*			k_0 *(iso)*			k_1 *(geo)*			k_2 *(vol)*		
DOY/SZA/RAA	*All*	*Back*	*Fwd*	*All*	*Back*	*Fwd*	*All*	*Back*	*Fwd*	*All*	*Back*	*Fwd*	*All*	*Back*	*Fwd*	*All*	*Back*	*Fwd*
156/50/10	0.19	0.29	0.19	0.02	0.17	0.02	0.51	0.06	0.26	0.25	0.38	0.25	0.02	0.22	0.03	0.70	0.12	0.35
156/43/14	0.18	0.05	0.18	−0.00	−0.23	0.02	0.68	1.34	0.34	0.24	−0.02	0.25	−0.01	−0.48	0.02	0.91	2.25	0.43
156/16/21	0.19	0.21	0.18	0.02	0.12	−0.00	0.65	1.52	0.68	0.25	0.27	0.24	0.02	0.13	0.01	0.75	1.76	0.58
156/09/79	0.19	0.19	0.19	0.01	0.00	−0.09	1.03	1.79	3.26	0.25	0.25	0.24	0.02	0.00	−0.14	1.13	2.10	4.50
220/65/14	0.10	0.10	0.09	0.01	0.01	0.01	0.23	0.21	0.23	0.20	0.23	0.15	−0.07	−0.05	−0.11	1.06	0.98	0.68
220/55/09	0.10	0.08	0.09	0.01	−0.00	0.01	0.28	0.34	0.19	0.20	0.07	0.18	−0.10	−0.25	−0.10	1.13	1.72	0.62
220/43/00	0.13	0.22	0.23	0.07	0.24	0.18	0.23	−0.29	2.01	0.20	0.51	0.20	−0.11	0.48	−0.09	1.14	−0.54	0.65
220/24/25	0.11	0.12	0.10	0.02	0.06	0.01	0.34	0.42	0.29	0.23	0.24	0.22	−0.06	−0.01	−0.07	0.82	0.92	0.79
220/23/29	0.08	0.09	0.08	0.00	0.03	0.00	0.27	0.34	0.22	0.19	0.20	0.19	−0.09	−0.04	−0.11	0.71	0.81	0.85
220/15/76	0.10	0.10	0.10	0.01	0.01	0.01	0.51	0.78	0.45	0.22	0.22	0.22	−0.05	−0.04	−0.09	0.74	0.38	1.68

All=both half-spaces; Back=backscattering only; Fwd=forward-scattering only; DOY=day of year; SZA=solar zenith angle; RAA=relative azimuth angle.

Table 7. Weights of Determination for Retrieved Parameters

Inner Mongolia Data Sets				*Arizona Data Sets*			
Sites	k_0	k_1	k_2	*DOY/SZA/RAA*	k_0	k_1	k_2
A2	1.1	2.8	67.9	156/50/10	3.8	5.6	150.0
A8	1.0	1.1	39.8	156/43/14	3.3	7.7	185.8
B9	1.0	2.5	75.9	156/16/21	0.8	7.1	346.2
C4	1.5	1.9	62.9	156/09/79	0.7	28.8	17398.3
D7	1.5	2.0	63.7	220/65/14	4.4	1.9	87.0
D8	1.2	0.8	34.1	220/55/09	4.1	4.1	125.6
F5	1.2	3.4	101.1	220/43/00	3.3	7.9	195.9
G9	1.8	3.5	81.7	220/24/25	1.4	8.2	239.3
Z	1.6	0.8	38.3	220/23/29	1.3	8.0	253.8
Y	0.6	0.1	6.9	220/15/76	0.9	10.8	4208.0

DOY=day of year; SZA=solar zenith angle; RAA=relative azimuth angle.

Table 8. Weights of Determination for Reflectance (Nadir Viewing at Mean Sun Angle of Observations) for Three Angular Distributions

Inner Mongolia				*Arizona*			
Sites	*All*	*Back*	*Fwd*	*DOY/SZA/RAA*	*All*	*Back*	*Fwd*
A2	0.111	3.982	0.402	156/50/10	0.249	0.974	0.867
A8	0.094	2.468	0.231	156/43/14	0.264	0.927	0.859
B9	0.218	1.061	0.288	156/16/21	0.296	0.906	0.793
C4	0.127	4.030	0.644	156/09/79	0.345	0.797	0.543
D7	0.114	2.972	0.391	220/65/14	0.227	0.934	0.877
D8	0.087	1.305	0.179	220/55/09	0.239	0.977	0.871
F5	0.116	0.407	0.294	220/43/00	0.264	0.559	0.860
G9	0.124	2.784	0.424	220/24/25	0.286	0.834	0.824
Z	0.101	1.584	0.211	220/23/29	0.290	0.850	0.819
Y	0.087	7.841	0.136	220/15/76	0.329	0.958	0.662

All=both half-spaces; Back=backscattering only; Fwd=forward-scattering only; DOY=day of year; SZA=solar zenith angle; RAA=relative azimuth angle.

number of observations but far less robust with respect to limited angular sampling; it is therefore appropriate for use with sparse angular reflectance datasets derived from wide-swath satellite observations, provided that observations in both forward and backward azimuthal sectors are available and that adequate care is taken to correct for the attenuating effects of the atmosphere, which contribute an angular signature to the signal that tends to dampen that of the surface (Rahman, 1996). The greatest hindrance to an adequate application of such a model to satellite data is the high probability of obtaining only a few cloud- and shadow-free observations. Attempts have been made to overcome this through the use of more than one sensor [e.g., the two Advanced Very High Resolution Radiometers (Chopping, 1999; Chopping, 1998a; Chopping, 1998b; Vives Ruiz de Lope and Lewis, 1997; Privette et al,. 1996)], although this is complicated by the lack of in-flight calibration for the solar channels. The future for multidirectional remote sensing and BRDF retrieval from space will be brighter with multiangular sensors and sensor combinations, such as MODIS and MISR on NASA's Terra satellite, as well as the simultaneous use of large field-of-view wide-swath/multiangular sensors on different platforms (SeaWiFS, AATSR, MODIS/MISR, VEGETATION, Global Land Imager, VIIRS on NPOESS).

The author would like to thank Bao Yin, Qin Shu Hui, and Saishee (Inner Mongolia Normal University, Hohhot) for invaluable help in acquiring the Xilingol grassland bidirectional reflectance dataset and Jiaguo Qi (Michigan State University, formerly of USDA-ARS Water Conservation Lab., Phoenix, Arizona) for supplying the Monsoon '90 data. Thanks are also extended to Professors Chen Shan (Inner Mongolia Normal University Biology Dept., Hohhot) and Yong Shi Peng (Inner Mongolia University Natural Resources Institute, Hohhot) for excellent advice on grassland communities and site selection. Thanks also to a number of other people, especially Jean-Louis Roujean (CNRM, Toulouse), Marc Leroy (CESBIO, Toulouse), and Wolfgang Lucht (PIK Potsdam, formerly of CRSA, Boston University), for their helpful advice and comments. Finally, the reviewers are thanked sincerely for their keen observations and suggestions on earlier drafts of the paper.

REFERENCES

Asner, G. P., Wessman, C. A., and Privette, J. (1997), Unmixing the directional reflectances of AVHRR subpixel land covers. *IEEE Trans. Geosc. Remote Sens.* 35(4):838–878.

Asner, G. P., Wessman, C. A., and Schimel, D. S. (1998), Heterogeneity of savanna canopy structure and function from imaging spectrometry and inverse modeling. Submitted to *Ecological Applications.* 8(4):1022–1036.

Barnsley, M. J., Allison, D., and Lewis, P. (1997a), On the infor-

mation content of multiple view angle (MVA) images. *Int. J. Remote Sens.* 18(9):1937–1960.

Barnsley, M., Lewis, P., Sutherland, M., and Muller, J.-P. (1997b), Estimating land surface albedo in the HAPEX-Sahel southern super-site: Inversion of two BRDF models against multiple angle ASAS data. *J. Hydrol.* 188–189:749–778.

Chopping, M. J. (1998a), The performance of linear semi-empirical BRDF models in a semi-arid grassland biome. In *Proceedings of the Remote Sensing Society Conference 1998: Developing International Connections*, Greenwich, England, 9–11 September 1998, pp. 568–574.

Chopping, M. J. (1998b), *Linear semi-empirical kernel-driven bidirectional reflectance distribution function models in monitoring semi-arid grasslands from space*, unpublished Ph.D. thesis, University of Nottingham, England, October 1998.

Chopping, M. J. (1999), Large-scale BRDF retrieval over New Mexico with a multiangular NOAA AVHRR dataset. *Remote Sens. Environ.* 74:164–192.

Curran, P. J., and Kupiec, J. A. (1995), Imaging spectrometry: A new tool for ecology. In *Advances in Environmental Remote Sensing* (F. M. Danson and S. E. Plummer, Eds.), John Wiley and Sons Ltd., Chichester, England.

Deering, D. W., and Leone, P. (1986), A sphere-scanning radiometer for rapid directional measurements of sky and ground radiance. *Remote Sens. Environ.* 19:1–24.

Deschamps, P.-Y., Bréon, F.-M., Leroy, M., Podaire, A., Bricaud, A., Buriez, J. C., and Sève, G. (1994), The POLDER Mission: Instrument characteristics and scientific objectives. *IEEE Trans. Geosc. Remote Sens.* 32:598–615.

Diner, D. J., Asner, G. P., Davies, R., Knyazikhin, Y., Muller, J.-P., Nolin, A. W., Pinty, B., Schaaf, C. B., and Stroeve, J. (1999), New directions in Earth observing: Scientific applications of multiangle remote sensing. *Bull. Am. Met. Soc.* 80(11):2209–2229.

Disney, M. I., and Lewis, P. (1998), An investigation of how linear BRDF models deal with the complex scattering processes encountered in a real canopy. In *Proceedings of the 1998 International Geoscience and Remote Sensing Symposium (IGARSS)*, 6–10 July, 1998, Seattle, WA, USA.

Disney, M., Lewis, P., Muller, J.-P., and Barnsley, M. J. (1997), Production and validation of BRDF and albedo extracted from airborne and spaceborne data. In *Physical Measurements and Signatures in Remote Sensing, Proceedings of the ISPRS Conference* (G. Guyot and T. Phulpin, Eds.), Courcheval, France, 7–11 April, 1997.

Engelsen, O., Pinty, B., Verstraete, M. M., and Martonchik, J. V. (1997), Design and evaluation of parametric bidirectional reflectance factor models. In *Physical Measurements and Signatures in Remote Sensing* (G. Guyot and T. Phulpin, Eds.), Balkema, Rotterdam, pp. 219–225.

Guyot, G. (1990), Optical properties of vegetation canopies. In *Applications of Remote Sensing in Agriculture* (M. D. Steven and J. A. Clark, Eds.), Butterworths, London, Boston.

Hautecoeur, O., and Leroy, M. M. (1998), Surface bidirectional reflectance distribution function observed at global scale by POLDER/ADEOS. submitted to *G.R.L.*, 2 June 1998. *Geophys. Res. Lett.* 25(22):4197–4200.

Hesley, Z., Barnsley, M. J., and Lewis, P. (1996), Estimating error in the retrieval of albedo (directional-hemispherical reflectance) under the combined angular sampling regime of the MODIS (AM) and MISR sensors. In *Proceedings of the 22nd Annual Conference of the Remote Sensing Society: Science and Industry*, *Remote Sensing Society*, Durham, England, 12–14 September 1996, pp. 537–542.

Hu, B., Lucht, W., Li, X., and Strahler, A. H. (1997). Validation of kernel-driven models for global modeling of bidirectional reflectance. *Remote Sens. Environ.* 62:201–214.

Huete, A. R., Hua, G., Qi, J., Chehbouni, A., and van Leeuwen, W. J. D. (1992), Normalization of multidirectional red and near-infrared reflectances with the SAVI. *Remote Sens. Environ.* 41:143–154.

Huete, A. R., Liu, H., de Lira, G. R., Batchily, K., and Escadafal, R. (1994), A soil color index to adjust for soil and litter noise in vegetation index imagery of arid regions. In *Surface and Atmosphere Remote Sensing: Technologies, Data Analysis and Interpretation, Proceedings of the 1994 International Geoscience and Remote Sensing Symposium*, Jet Propulsion Laboratory, California Institute of Technology, Pasadena, CA, 8–12 August, 1994.

Hyman, A. H., and Wanner, W. (1997), Relationships between semi-empirical BRDF model parameters and land cover type. In *Developing Space '97, Proceedings of the 1997 Remote Sensing Society Annual Student Meeting*, University College London, England, 17 April 1997, pp. 30–35.

Iaquinta, J., and Fouilloux, A. (1998), Influence of the heterogeneity and topography of vegetated land surfaces for remote sensing applications. *Int. J. Remote Sens.* 19(9):1711–1723.

Jackson, R. D., Moran, S., Slater, P. S., and Biggar, S. F. (1987), Field calibration of reference reflectance panels. *Remote Sens. Environ.* 22:145–158.

Jackson, R. D., Teillet, P. M., Slater, P. N., Fedosejevs, G., Jasinski, M. F., Aase, J. K., and Moran, M. S. (1990), Bidirectional measurements of surface reflectance for view angle corrections of oblique imagery. *Remote Sens. Environ.* 32:189–202.

Kimes, D. S. (1983), Dynamics of directional reflectance factor distribution for vegetation canopies. *Applied Optics* 22(9):1364–1372.

Kimes, D. S., Newcombe, W. W., Nelson, R. F., and Schutt, J. B. (1986), Directional reflectance distributions of a hardwood and a pine forest canopy. *IEEE Trans. Geosci. Remote Sens.* GE-24(2):281–293.

Kimes, D. S., Newcombe, W. W., Tucker, C. J., Zonnefeld, I. S., van Wijngaarden, W., de Leeuw, J., and Epema, G. F. (1985), Directional reflectance factor distributions for cover types of Northern Africa. *Remote Sens. Environ.* 18:1–19.

Kmenta, J. (1986), *Elements of Econometrics*, Macmillan, New York.

Kustas, W. P., and Goodrich, D. C. (1994), Preface to Water Resources Research Special Monsoon '90 edition. *Water Resources Research* 30(5):1271–1279.

Kuusk, A. (1991), The hotspot effect in plant canopy reflectance. In *Photon-Vegetation Interactions, Applications in Optical Remote Sensing and Plant Ecology* (Myneni, R. B. and Ross, J., Eds.), Springer-Verlag, Berlin, pp. 139–159.

Leroy, M., and Bréon, F.-M. (1996), Angular signatures of surface reflectances from airborne POLDER data. *Remote Sens. Environ.* 57:97–107.

Lewis, P., Disney, M. I., Barnsley, M. J., and Muller, J.-P. (1998), Deriving albedo maps for HAPEX-Sahel from ASAS data using kernel-driven BRDF models. Submitted for publication in *Hydrology and Earth System Sciences. 1999. Hydrology and Earth System Sciences* 3(1):1–13.

Lewis, P., and Wanner, W. (1996), Progress report: Noise sensitivity of BRDF and albedo retrieval from the Earth Observing

System MODIS and MISR sensors with respect to angular sampling. In *MODIS BRDF/Albedo Product: Algorithm Theoretical Basis Document Version 4.0* (A. H. Strahler, W. Wanner, C. B. Schaaf, X. Li, B. Hu, J.-P. Muller, P. Lewis, and M. J. Barnsley, Eds.), NASA/GSFC, MODIS Product ID: MOD43, November 1996 (Appendix C).

Li, X., Strahler, A. H., and Woodcock, C. (1994), A hybrid geometric-optical radiative-transfer model for directional reflectance of discontinuous vegetation canopies. In *Surface and Atmosphere Remote Sensing: Technologies, Data Analysis and Interpretation, Proceedings of the 1994 International Geoscience and Remote Sensing Symposium (IGARSS)*, Jet Propulsion Laboratory, CALTECH Pasadena, CA, 8–12 August, 1994.

Li, Z., Cihlar, J., Zheng, X., Moreau, L., and Ly, H. (1996), The bidirectional effects of AVHRR measurements over Boreal Regions. *IEEE Trans. Geosci. Remote Sens.* 34(6):1308–1322.

Middleton, E. M., Deering, D. W., and Ahmad, S. P. (1987), Surface anisotropy and hemispheric reflectance for a semiarid ecosystem. *Remote Sens. Environ.* 23:193–212.

Moran, M. S., Clarke, T. R., Kustas, W., Weltz, M., and Amer, S. (1994), Evaluation of hydrologic parameters in a semiarid rangeland using remotely-sensed spectral data. *Water Resources Research* 30(5):1287–1297.

Notes for Users (Anonymous) (1993), *Milton Multiband Radiometer Notes for Users Version 5*, December 1993, NERC Pool for Field Spectroscopy (author unknown).

Pinty, B., and Verstraete, M. (1991), Extracting information on surface properties from bidirectional reflectance measurements. *J. Geophys. Res.* 96(D2):2865–2874.

Privette, J. L., Deering, D. W., and Wickland D. E. (1997), *Report on the Workshop on Multiangular Remote Sensing for Environmental Applications* (Jan. 29–31, 1997), workshop sponsored by the NASA Terrestrial Ecology Programme, NASA Technical Memorandum 113202.

Privette, J. L., Emery, W. J., and Schimel, D. S. (1996), Inversion of a vegetation reflectance model with NOAA AVHRR data. *Remote Sens. Environ.* 58:187–200.

Qi, J., Cabot, F., Moran, M. S., and Dedieu, G. (1995), Biophysical parameter estimation using multidirectional spectral measurements. *Remote Sens. Environ.* 54:71–83.

Qi, J., Huete, A. R., Cabot, F., and Chehbouni, A. (1994), Bidirectional properties and utilizations of high-resolution spectra from a semiarid watershed. *Water Resources Research* 30(5):1271–1279.

Rahman, H. (1996), Atmospheric optical depth and water vapour effects on the angular characteristics of surface reflectance in NOAA AVHRR. *Int. J. Remote Sens.* 17(15):2981–2999.

Rollin, E. M., Emery, D. R., and Milton, E. J. (1996), Reference panel anisotropy in field spectroscopy. In *Proceedings of the 22nd Annual Conference of the Remote Sensing Society: Science and Industry*, Durham, England, 12–14 September 1996, pp. 602–609.

Rondeaux, G. (1990), *Polarisation de la lumière réfléchie par un couvert végétal*, Doctoral thesis, University Paris VII, June 1990.

Ross, J. (1981), *The Radiation Regime and Architecture of Plant Stands*, Dr. W. Junk Publishers, The Hague, Netherlands.

Roujean, J.-L., Leroy, M., and Deschamps, P.-Y. (1992a), A bidirectional reflectance model of the Earth's surface for the correction of remote sensing data. *J. Geophys. Res.* 97(D18):20,455–20,468.

Roujean, J.-L., Leroy, M., Podaire, A., and Deschamps, P.-Y. (1992b), Evidence of surface reflectance bidirectional effects from a NOAA/AVHRR multi-temporal data set. *Int. J. Remote Sens.* 13(4):685–698.

Roujean, J.-L., Tanré, D., Bréon, F.-M., and Deuzé, J.-L. (1997), Retrieval of land surface parameters from airborne POLDER bidirectional reflectance distribution function during HAPEX-Sahel. *J. Geophys. Res.* 102(D10):11201–11218.

Sandmeier, S., and Itten, K. I. (1999), A field goniometer system (FIGOS) for acquisition of hyperspectral BRDF data. *IEEE Transact. Geosci. Remote Sens.* 37(2):978–986.

Schaaf, C. B., Li, X., and Strahler, A. H. (1994), Validation of canopy bidirectional reflectance models With ASAS imagery of a spruce forest in Maine. In *Surface and Atmosphere Remote Sensing: Technologies, Data Analysis and Interpretation, Proceedings of the 1994 International Geoscience and Remote Sensing Symposium (IGARSS)*, Jet Propulsion Laboratory, California Institute of Technology, Pasadena, CA, 8–12 August, 1994.

Schlesinger, W. H., Reynolds, J. F., Cunningham, G. L., Huenneke, L. F., Jarrell, W. M., Virginia, R. A., and Whitford, W. G. (1990):Biological feedbacks in global desertification. *Science* 247:1043–1048.

Strahler, A. H., Wanner, W., Schaaf, C. B., Li, X., Hu, B., Muller, J.-P., Lewis, P., and Barnsley, M. J. (1996), *MODIS BRDF/Albedo Product: Algorithm Theoretical Basis Document Version 4.0*, NASA/GSFC, MODIS Product ID: MOD43, November 1996.

Takemata, K., Shimizu, S., and Kawata, Y. (1999), Estimation of bidirectional reflectance distribution function from land surfaces using ADEOS/POLDER image data. In *Remote Sensing of the Earth–A Challenge for the 21st Century: Proceedings of the 1999 International Geoscience and Remote Sensing Symposium (IGARSS)*, 28 June–2 July 1999, Hamburg, Germany, pp. 1096–1098.

Vives Ruiz de Lope, E., and Lewis, P. E. (1997), Monitoring land surface dynamics in the HAPEX Sahel area using kernel driven BRDF models and AVHRR data. In *Physical Measurements and Signatures in Remote Sensing, Proceedings of the ISPRS Conference* (G. Guyot and T. Phulpin, Eds.), Courcheval, France, 7–11 April, 1997.

Walthall, C. L. (1997), A study of reflectance anisotropy and canopy structure using a simple empirical model. *Remote Sens. Environ.* 61:118–128.

Walthall, C. L., Norman, J. M., Welles, J. M., Campbell, G., and Blad, B. L. (1985), Simple equation to approximate the bidirectional reflectance from vegetative canopies and bare surfaces. *Applied Optics* 24(3):383–387.

Wanner, W., Li, X., and Strahler, A. H. (1995), On the derivation of kernels for kernel-driven models of bidirectional reflectance. *J. Geophys. Res.* 100:21077–21090.

Wu, A., Li, Z., and Cihlar, J. (1995), Effects of land cover type and greenness on Advanced Very High Resolution Radiometer bidirectional reflectances: Analysis and removal. *J. Geophys. Res.* 100(D5):9197–9192.

Xiao, X., Ojima, D. S., and Bonham, C. D. (1993), *Regional climate-vegetation-soil patterns of Inner Mongolia, China*, paper presented at the 1993 conference on Grassland Ecosystem of the Mongolian Steppe (GEMS), Racine, WI, USA.